12-9-2016 12:00 AM

Properties of High Nitrogen Content Carbon Nitride Thin Films Prepared by a Radio Frequency Magnetron Sputtering Deposition Technique

David Pipher
The University of Western Ontario

Supervisor
Dr. Oleg Semenikhin
The University of Western Ontario

Graduate Program in Chemistry
A thesis submitted in partial fulfillment of the requirements for the degree in Master of Science
© David Pipher 2016

Recommended Citation
Pipher, David, "Properties of High Nitrogen Content Carbon Nitride Thin Films Prepared by a Radio Frequency Magnetron Sputtering Deposition Technique" (2016). *Electronic Thesis and Dissertation Repository*. 4318.
https://ir.lib.uwo.ca/etd/4318

Abstract

The properties of carbon nitride (CNx) films deposited onto various substrates using a radiofrequency magnetron sputtering technique were studied as a function of deposition parameters, especially magnetron power, gas pressure and nitrogen content in the plasma. Indium tin oxide (ITO) coated glass and fluorine tin oxide (FTO) coated glass as well as metal substrates (silver and tungsten) were used. Scanning electron microscopy (SEM) was used to study the surface morphology of the prepared CNx films. Energy-dispersive X-ray spectroscopy (EDX) as well as survey X-ray photoelectron spectroscopy (XPS) spectra were used to perform the elemental analysis of the CNx films.

Ultraviolet-visible (UV-Vis) spectrophotometry was conducted to study CNx films on ITO glass to characterize the absorption spectrum and thickness of the film, as well as estimate the material's band gap. Schottky cells were created using either ITO or FTO coated glass as the substrate, CNx films as the active material, and aluminum as the counter electrode. Current-voltage, current-time, and voltage-time plots were used to demonstrate the photovoltaic effect in the samples, as well as to show the benefits of ageing and annealing to the cell's performance.

Different annealing conditions were explored to try and remove the high levels of oxygen that were found in the CNx films in an attempt to increase the open circuit voltage of the cells. It was concluded that oxygen comes from conducting metal oxides (ITO/FTO) during the film deposition process. Therefore, metal contacts (silver and tungsten) were subsequently used instead of ITO or FTO glass which resulted in low oxygen CNx films.

The bonding patterns in CNx films were determined using high-resolution XPS as a function of deposition parameters as well as annealing. It was found that the films contained a significant amount of pyridinic moieties, which increased upon annealing. On the contrary, the contribution of quaternary nitrogen, which is the main n-doping configuration in carbon nitride, was quite small and further decreased with annealing. The XPS results allowed us to shed light on the nature of photoactivity demonstrated by high nitrogen content carbon nitride films.

Keywords: Amorphous Carbon Nitride, Photovoltaic Effect, Bonding Patterns, Photoconductivity, N-type Semiconductor

Acknowledgements

I would like to start out by thanking my supervisor, Dr. Oleg Semenikhin, for his support throughout my unconventional path towards my degree. Despite different struggles, his guidance and encouragement was crucial to the eventual completion of my thesis. I want to thank my fellow graduate students from the Semenikhin Lab, Mike Nieradko and Ladan Eskandarian, who provided much needed help throughout my degree. I want to thank Dr. Mark Biesinger for his advice and quick turnaround of samples that needed to be analyzed. Finally, I could not have made it to the completion of my degree without the unconditional support from my friends and family.

Table of Contents

List of Tables

List of Figures

Symbols and Acronyms

EDX	Energy Dispersive X-ray
SEM	Scanning Electron Microscope
CNx	Carbon Nitride
a-CNx	Graphitic Amorphous Carbon Nitride
ta-CNx	Diamond-like Amorphous Carbon Nitride
XPS	X-Ray Photoelectron Spectroscopy
r.f	Radio Frequency
DC	Direct Current
ITO	Indium Tin Oxide
FTO	Fluorine Tin Oxide
UV-Vis	Ultraviolet-Visible
a-C	Amorphous Carbon
$g\text{-}C_3N_4$	Graphitic Carbon Nitride
ta-C	Diamond-like Amorphous Carbon
J-V	Current-Voltage
I-t	Current-Time
FF	Fill Factor
V_{OC}	Open Circuit Voltage
I_{SC}	Short Circuit Current
I_{max}	Photocurrent at Maximum Power
V_{max}	Voltage at Maximum Power
P_{in}	Input Power
P_{max}	Maximum Power Attainable
η_e	Power Conversion Efficiency

Chapter 1 : Introduction

1.1 Background

1.1.1 Amorphous Carbon and Carbon Nitride Thin Films

Diamond and graphite are the two most common allotropes of carbon, and have very different properties. Diamond is isotropic and made up of sp^3 covalent bonds in a tetrahedral network. Graphite is anisotropic and is composed of stacks of sp^2 graphene sheets. Graphite is opaque, soft, and has weak interactions between the stacked graphene sheets that make up its composition. It is also a good conductor and its opaque nature is visual proof that it absorbs visual light. In contrast to this, diamond is very hard, transparent, an insulator and reflects visible light. Amorphous carbon is a class of compounds that are defined by how much of their composition is derived from sp^3 bonds, as in diamond, and from sp^2 bonds, as in graphite [1]. Diamond-like amorphous carbon (ta-C) has $80 - 85\%$ sp^3 bonding and is an insulator. However, due to the sp^2 bonding present, the bandgap is lower than that of diamond because of the increased π and π^* states. Graphitic amorphous carbon (a-C) has around 95% sp^2 bonds, and is a semi-metal similar to graphite but lacks the same long range order. Instead, it is made up of graphitic islands that range from $15 - 20$ Å in diameter [2]. The relative amounts of sp^2 and sp^3 regions in the a-C films will determine the different physical and chemical properties. These properties include film hardness, transparency, conductivity and electrochemical reactivity. The sp^2 regions control the electronic and optical properties which is especially important for photovoltaic applications.

It is possible to control the electronic properties of the carbon films by doping them with different heteroatoms, such as boron, nitrogen, phosphorous, or sulfur. Boron doped diamond is a well studied doped carbon film that has potential applications in electrochemistry [3]. The addition of boron leads to p-type doping because of the one fewer valence electron that boron has compared to carbon. When nitrogen is incorporated into amorphous carbon, you create an interesting group of materials called carbon nitride (CNx). The incorporation of nitrogen into CNx modifies the film considerably, changing the nature of its π and π^* states [4]. If nitrogen is doped into amorphous carbon with mainly sp^3 bonding (ta-C), you form an insulating form of carbon nitride (ta-CNx). Originally, ta-C is an insulator with no π or π^* states but incorporating nitrogen introduces sp^2 states. This increases conductivity and can also decrease the optical bandgap if enough nitrogen is incorporated. The doping effects of ta-CNx are different depending on how much nitrogen is

incorporated. Low nitrogen doping levels are defined as less than 2% and are termed as σ doping. As nitrogen content increases in the low nitrogen domain, the Fermi level rises from above the valence band to just below the conduction band. This results in an increase in conductivity because of the decrease in activation energy resulting from the Fermi level being close to the conduction band. For the low nitrogen doping levels, the optical gap and relative sp^3 bonding remains the same [5]. High nitrogen doping levels are defined as >2% and are termed as π doping. For high nitrogen doping, sp^2 bonding increases and sp^3 bonding decreases, and the electronic properties are governed by the sp^2 bonding.

Despite ta-CNx being an interesting class of compounds and demonstrating how nitrogen doping can affect the electronic properties of a CNx film, they are generally too insulating and do not absorb visible light which prevents them from being studied for applications in solar cells. If nitrogen is incorporated into amorphous carbon with primarily sp^2 bonding (a-C), you will form either a conductive or semiconducting form of carbon nitride (a-CNx) [6]. Bonding in CNx films is varied and complex due to the large number of chemical environments nitrogen and carbon can participate in [7]. Figure 1-1 shows the different bonding configurations that can be found in a CNx film.
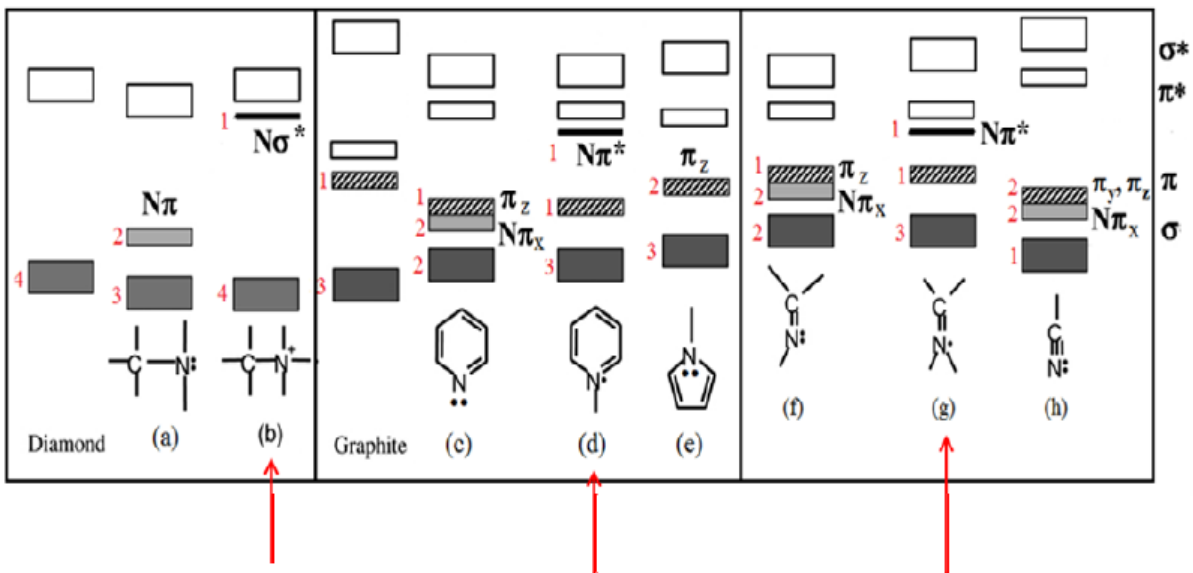
Figure 1-1: A summary of the different bonding configurations possible between carbon and nitrogen with their valence and conduction band energies. The red numbers indicate the number of valence electrons occupying each level. Modified from ref. 10.

Bonding formations (a) and (b) relate to diamond films with no or little π-bonding and thus are not relevant for CNx studied in this work. Bonding formation (c) is pyridinic, (d) is quaternary, (e) is pyrrolic, and all of them are semiconductors compared to graphite because of the increased bandgap. Bonding formations (f) and (g) are semiconductors, and (h) is insulating because of its increased bandgap [8]. Of these configurations, (d) and (g) are n-doping configurations, the rest are intrinsic semiconductors [2]. Bonding formations (b), (d) and (g) are indicated with the red arrows in the figure.

When nitrogen is bonded to carbon and still has an extra electron, it can participate in doping, resulting in a semiconductor with n-type properties. However, for this to happen, the electron should be able to conjugate with other electrons of the graphitic network. Overall, CNx films mainly have pyridinic, pyrrolic and quaternary bonding patterns, indicated by (c), (e) and (d), respectively. Pyridinic and pyrrolic moieties cannot contribute to n-type doping because they have three valence electrons participating in sp^2 hybridization to form bonds with carbon, and two valence electrons to form a lone pair in a p orbital. The lone pair is located out of plane with graphitic π electrons for pyridinic moieties or is involved in formation of aromatic structure in case of pyrrolic moieties and thus does not contribute to conductivity. Quaternary nitrogen (d) does contribute to n-type doping because it has three valence electrons to form σ bonds with carbon, one valence electron in the π state and an extra valence electron to occupy the π^* state. Carbon provides the other valence electron to fill the π state thus forcing the second electron from the nitrogen lone pair to go into the π^* orbital. Therefore, the concentration of electrons in the graphitic π-electron system increases.

The other two main bonding configurations (c) and (e), will not contribute to conductivity. Furthermore, since the pyridinic moieties (c) cannot fit in the same plane as the graphitic domains formed by carbon and quaternary nitrogen, they will be breaking up the graphitic pathways that cause the films to be conducting. For this to happen, there must be a significant fraction of nitrogen in the film in the first place; otherwise, we should expect to see highly conducting films due to mainly pure graphitic domains with no nitrogen incorporation. Furthermore, the deposition conditions should allow formation of pyridinic bonding configurations that will break up the extended graphitic network and make the CNx films semiconductors. Doping with a small amount

of nitrogen may increase the conductivity of a-C by supplying and populating more π and π^* states. This will make such films unsuitable for photovoltaic applications.

The characterization of bonding in CNx films has been a challenge within the scientific community. This is for several reasons, including the similar energies and shifts of C-C and C-N bonds, and the broad peaks in spectra due to the highly amorphous nature of most CNx films [2]. High-resolution X-Ray photoelectron spectroscopy (XPS) is used to determine the different bonding patterns in the films prepared in this work. In this research, a-CNx films are being studied and therefore for the ease of the reader it will be referred to simply as CNx for the rest of the thesis.

There has been limited research on the electronic properties of n-type materials like CNx, as most papers have been focused on their interesting mechanical properties [9]. Novel work on CNx films with very high nitrogen incorporation has recently been done within our group [10]. The goal is to increase the % N_2 in the CNx film which results in more aromatic bonding. At a high enough nitrogen content, the CNx films transitions from a semi-metal to a semiconducting CNx film [6,11]. Ideally nitrogen will act as an n-type dopant, resulting in an n-type semiconductor with applications in photovoltaic cells. Increasing the nitrogen content in the CNx films increases thickness but also induces stress in the film [12]. CNx films that are freshly deposited will also have a high degree of stress and disorder. This is a combination of tensile stress from the deposition procedure and the incorporation of nitrogen and oxygen atoms [13,14]. CNx films undergo film relaxation over time, resulting in structural modification. Annealing at a reasonable temperature can help this relaxation process by changing the bonding structure [15]. The deposition conditions also have a profound impact on the properties of the CNx film, as well as the nitrogen content found in the prepared film, as discussed in the next section.

Since different bonding patterns will result in different chemical environments for nitrogen and carbon atoms in the films, they can be distinguished and analyzed by using a technique such as XPS. The details regarding bonding patterns and binding energies found in CNx films will be discussed below.

1.1.2 Preparation of CNx Thins Films

There are many different techniques to prepare CNx films, including ion-beam deposition, laser techniques, and chemical vapour deposition processes. High energy techniques like vacuum cathodic arc deposition preferentially deposits an insulating tetrahedral carbon nitride film, ta-CNx, which is unfavourable for the work in this thesis. Direct current (DC) and radio frequency (r.f) magnetron sputtering deposition is a low energy, high throughput process that can create a variety of different types of conducting and semiconducting carbon nitride films, such as a-CNx [16]. The technique used for all the work conducted in this report was r.f magnetron deposition. A schematic of the vacuum deposition chamber can be seen in Figure 1-2.
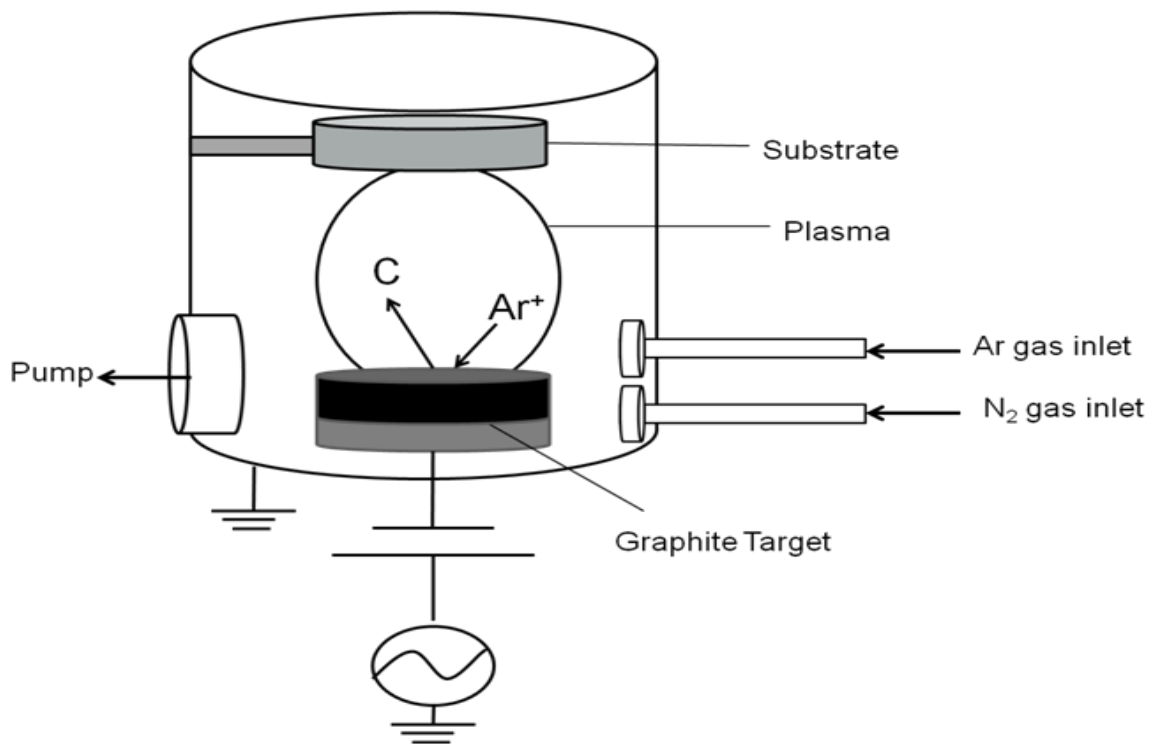
Figure 1-2: Schematic of the vacuum deposition chamber.

When gas enters the chamber, a certain percentage of the molecules will become ionized, creating a plasma. A magnetron located behind the target focuses the plasma near the target surface to promote collisions. Due to the large electric field created by the negative bias applied to the target, the ions bombard the target. This relies on momentum transfer of the ions to deposit the ejected material from the target onto the substrate. The ions can be either argon or nitrogen, depending

on the deposition required. Using argon results in non-reactive deposition, while nitrogen reacts with a graphite target, producing a CNx film on the substrate. There can also be a mix of nitrogen and argon gas which produces a CNx film with different properties, as will be discussed later. The actual setup of the deposition equipment, along with a visual representation of the plasma, can be seen in Figure 1-3.

Ar Plasma   Ar + N_2 Plasma
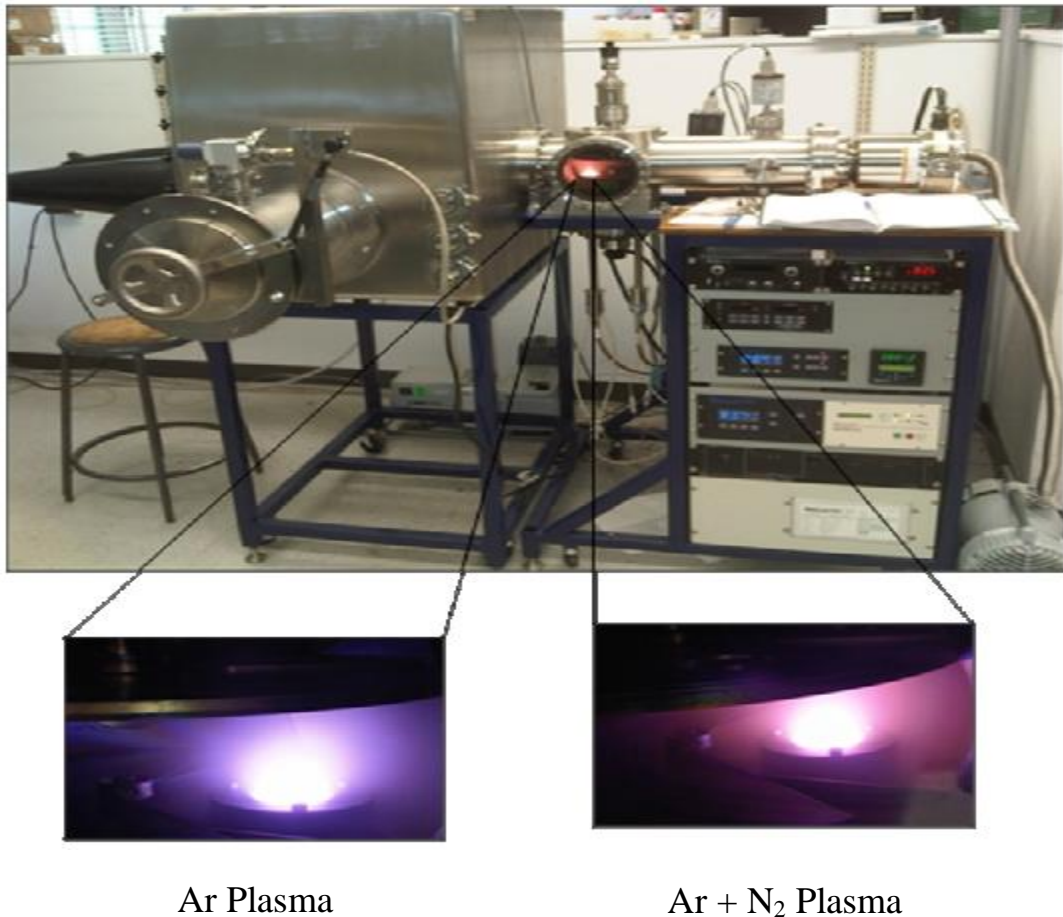
Figure 1-3: Custom built magnetron sputtering deposition equipment. Two different types of plasma are shown close-up, a pure argon plasma on the left and a mix of argon and nitrogen plasma on the right.

There are many different parameters involved in the deposition process that have a large effect on the type and quality of films formed. These parameters include deposition pressure, time, power, and % of N_2 gas in the chamber. Deposition time has a straightforward effect on the CNx film created, with the film thickness increasing as the deposition time increases. The other three

parameters have more complex and subtle effects on the nature of the final deposited CNx film. The % of N_2 in the chamber is calculated from the formula:

$$\%N_2 = \frac{Flow\ Rate\ of\ N_2}{Flow\ Rate\ of\ N_2 + Flow\ Rate\ of\ Ar} * 100\% \tag{1}$$

It is important to note that this is the % of N_2 gas in the chamber and not how much nitrogen will end up in the deposited CNx film. In fact, the data obtained in this thesis suggest that the nitrogen content in the films remains approximately the same when the nitrogen concentration in the plasma exceeds a certain threshold. This was particularly seen from conductivity measurements and UV-Vis spectra that showed similar values for samples prepared at 75% and 100% N_2 gas, as well as XPS data, as discussed later. Increasing the deposition power has been found in the literature to result in less nitrogen being incorporated into the deposited CNx film. This is because the kinetic energy of the bombarding species increases with the deposition power. The increased energy results in chemical resputtering of the growing CNx film on the substrate. Nitrogen is preferentially displaced as compared to carbon, and as a result there is less nitrogen in the final deposited CNx film [17]. Also, lower deposition power should favor the formation of more complex aromatic and π-conjugated bonding configurations. Because of these considerations and our desire to prepare films with high nitrogen content and better semiconducting properties, we used mostly low powers of 25 and 50 W in this thesis. Despite less nitrogen being incorporated into the film, the film thickness increases linearly with increasing deposition power [18]. Increasing power also increases stress and disorder in the CNx films, which can result in delamination of the film in solution [19]. On the contrary, increasing deposition pressure can help incorporate more nitrogen into the sample. A higher pressure increases the likelihood that the nitrogen gas will react with the carbon atoms in the plasma, producing more nitrogen rich CNx films. An increased pressure also lowers the mean free path of the ejected CN species, raising the possibility of more reactive steps on the path towards the substrate [20]. This should produce more complex nitrogen-containing moieties. This was also tested in our XPS experiments. Increasing the deposition temperature was not explored, as it has been to shown to decrease nitrogen content in the film [21].

1.1.3 Photoactivity and the Schottky Design

Conductors are a class of material that do not experience an increase in the amount of charge carriers when they are exposed to light. Semiconductors can display two different types of photoactivity: photoconductivity and the photovoltaic effect. Photoconductivity is when the amount of charge carriers (electrons and holes) increases when the semiconductor is exposed to light, but the charge carriers can move in both directions and be collected at either electrode, which results in no power being generated. The photovoltaic effect is similar to photoconductivity but the charge carriers can not move in both directions, which results in the electrons being collected at one electrode and the holes being collected at the other, and power is generated. The latter is the effect necessary for a working solar cell. The simplest design for a Schottky cell is a semiconductor layer sandwiched between glass (usually ITO or FTO) and a metal electrode that has a different work function than the glass. This difference promotes charge separation at the interfaces. This is called a Schottky device since there is no p-n junction and the carriers are separated at the interfaces between the semiconductor and the contacts. The active layer in our design is CNx which is responsible for producing the photoinduced charge. If the charge separation is successful, the excited electron will be extracted at the metal electrode which acts as the cathode, and the hole will be extracted at the ITO/FTO glass, which is the anode. It is important for CNx to have an absorption spectra that has its maximum in the UV-VIS range to be applicable in a solar cell. In addition, CNx must have only one type of photogenerated charge carrier, either electrons or holes, to produce the photocurrent. If both types are created recombination will occur and the cell will not show promising photovoltaic properties. We expected CNx to be an n-type semiconductor as described above. Therefore, the photocurrent would be generated by the flux of photogenerated holes, which act as the minority carrier in this case. Finally, the charge carrier mobility must be high within the CNx film to prevent recombination before the carriers can be collected at the electrodes.

The Schottky cell was the design used for all cell samples, as shown in Figure 1-4. The CNx-Al layer was held constant for all Schottky cells made. The Schottky designs used in this thesis consist of a glass layer (ITO or FTO), followed by a CNx film, and finally an aluminum contact. When a light source was shone onto the CNx layer through the non-conductive side of the glass at the location where the aluminum keyhole had been deposited on the conductive side,

photo excited holes were generated and extracted from the CNx film to the conductive ITO layer. The electrons could then travel through the aluminum keyhole, through the fully deposited portion, and be collected at the gold electrode contacting the aluminum film.
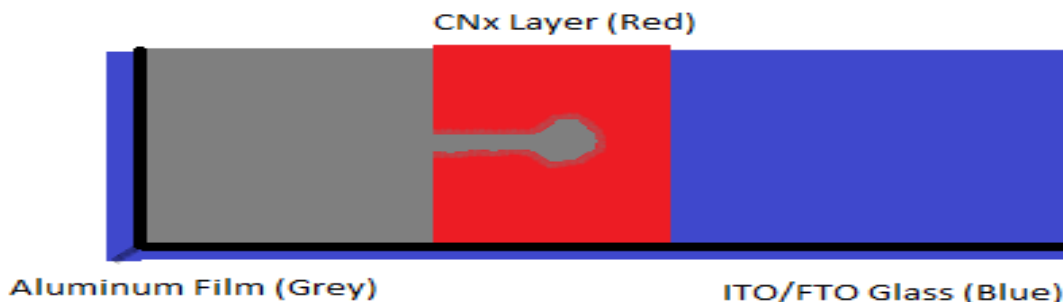
Figure 1-4: Schottky architecture used for prepared samples.

1.1.4 Current-Voltage Plots

Current-voltage (J-V) measurements are a standard technique that ramps the potential of the working electrode and measures the resulting current at the working electrode. In the case of the prepared Schottky cells, the working electrode is the ITO/FTO glass. This technique is useful because it gives a value of both the open circuit potential, as well as the short circuit current, when the cell is exposed to light. A standard J-V plot for a semiconductor is shown in Figure 1-5. The open circuit potential (V_{OC}) is defined as the difference in electrode potential of a system when there is no current in the system, and can be found as the x-intercept on a J-V graph. The short circuit current (I_{SC}) is defined as the current of a system when the voltage across is 0, and be found as the y-intercept on a J-V graph.
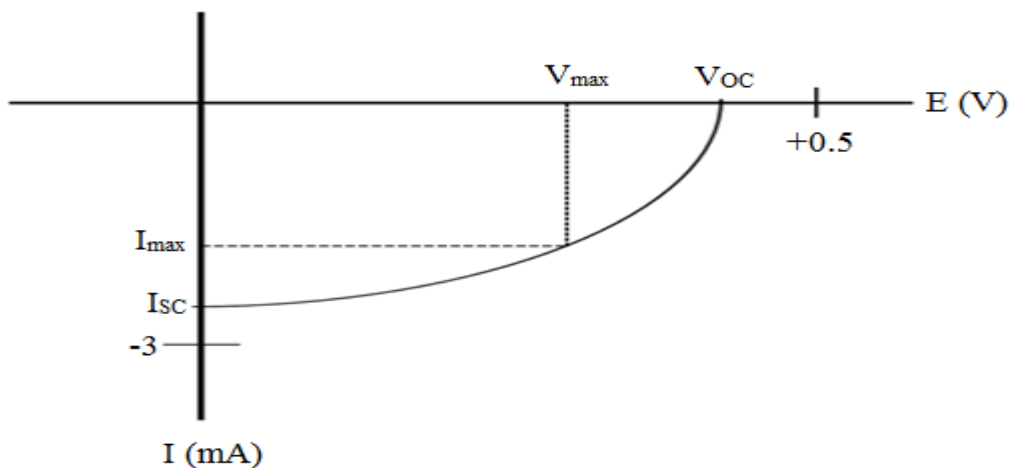
Figure 1-5: A typical J-V plot showing the important parameters: V_{OC}, I_{SC}, I_{max}, and V_{max}.

9

I_{max} and V_{max} are the maximum current and voltage that can be generated from the cell, respectively. The maximum power attainable from the cell (P_{max}) can be calculated as follows:

$$P_{max} = V_{max} * I_{max} \tag{2}$$

Another important parameter is the fill factor (FF), a measure of how close the maximum power of the cell is to the product of the open circuit potential and the short circuit current:

$$FF = \frac{I_{max}V_{max}}{V_{OC}I_{SC}} \tag{3}$$

A higher fill factor means the cell is more efficient. Once the input power is determined, P_{in}, the power conversion efficiency of a cell (η_e) can be calculated as:

$$\eta_e = \frac{V_{OC}I_{SC}FF}{P_{in}} \tag{4}$$

1.1.5 Voltage-Time Plots

These graphs plot the open circuit voltage of a cell as a function of time. This type of graph is useful to demonstrate that the cell is indeed a photovoltaic one. Specifically, that it can generate a photovoltage and therefore the photocurrent generation is due to the photovoltaic effect. For instance, photocurrent could be also produced by a change in the cell resistance upon illumination. This mechanism is called photoconductivity; however, a photoconductive device cannot generate photovoltage since there is no charge separation in this case, only change in the carrier concentration. These plots are also interesting because they allow one to observe transient processes occurring when the sample is exposed on and off to a light source. Finally, the occurrence of an open circuit photovoltage is a good initial test to see if there is a short circuit in the prepared cell.

1.1.6 X-Ray Photoelectron Spectroscopy (XPS)

XPS provides valuable insight into the different bonding configurations in high nitrogen content CNx films [22]. XPS analyzes the surface of the material but it has been shown that the surface bonding patterns are representative of the bulk material in CNx films [23]. The XPS survey spectra are used to determine the elemental composition of the sample; however, much more interesting

information can be provided by high-resolution XPS spectra that analyze relatively minor changes of the binding energy of an element due to changes in the chemical environment.

1.1.6.1 Carbon 1s high resolution XPS

Due to the many different bonding environments carbon can participate in, there is usually one large broad peak in the C 1s spectrum [7]. This peak usually comprises four main components. The one with the lowest binding energy is that of graphitic carbon (C-C and C=C bonds) located at approximately 284.5 eV. As more nitrogen is incorporated into the film, two components at higher binding energies in the C 1s spectrum become evident because of the higher electronegativity of nitrogen. Carbon atoms bound to so-called pyridinic nitrogen produce a signal in carbon C1s spectra at ca. 286 eV, whereas carbon bound to pyrrolic nitrogen produces a signal at ca. 288 eV. In addition, one can usually detect an additional peak due to so-called π-π* (shake-up) effect at ca. 290.9 eV due to valence electrons of the aromatic rings being excited by emitted photoelectrons.

1.1.6.2 Nitrogen 1s high resolution XPS

Despite the patterns revealed by the high-resolution carbon 1s XPS data, the bonding patterns found for nitrogen are more fundamental to our discussion. The main nitrogen groups found in carbonaceous materials are associated with so called pyrrolic, pyridinic and quaternary nitrogen, as shown in Figure 1-6 [24]. Pyrrolic bonding is when nitrogen is in a pyrrole 5-member ring type configuration, where its lone pair of π-electrons are donated to the aromatic system. Pyridinic bonding is when nitrogen is in a pyridine type 6-member ring configuration, where its lone pair is not part of the aromatic system. Quaternary bonding, also called graphitic bonding, is when nitrogen is substituted into the graphitic network [25].
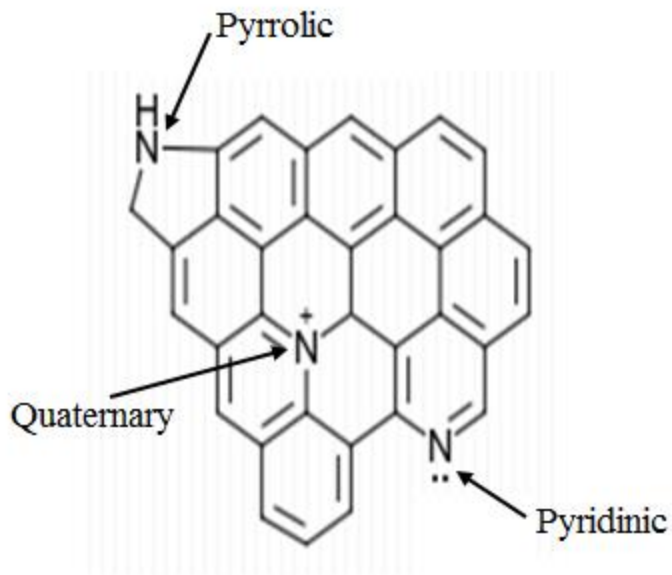
Figure 1-6: Different bonding environments for nitrogen in CNx films.

These bonding patterns have shown to have a wide range of binding energies depending on how the materials are synthesized or deposited. Pyridinic peaks usually appear in between 398.1 – 399.3 eV, pyrrolic peaks around 399.8 – 401.2 eV, and quaternary peaks around 401.1 – 402.7 eV [26,27]. Although pyrrolic, pyridinic and quaternary are the three main bonding configurations, Figure 1-7 shows other possible bonding patterns for nitrogen in CNx films. Pyridonic and nitrosic bonding could play a small part in the pyrrolic peak, but this would be minimal due to the small oxygen content in the film. The ammonium bonding configuration could contribute to the quaternary peak, and the amine bonding configuration could contribute to the pyridinic peak. The pyridine-N-oxide and nitro binding energies were not seen on the XPS data and therefore are not considered in the different bonding configurations of the CNx films in this work.

Pyrrole · · · Pyridine · Pyridinium · Pyridone · · · Pyridine-N-oxide

400.4 eV · 398.9 eV · 401.2 eV · · 400.6 eV · · · 403.2 eV

Amine · · · · Ammonium · Nitro · · · · · Nitroso · · Cyano

399.4 eV · · 401.5 eV · · · 406.1 eV · · · 400.1 eV · 399.5 eV
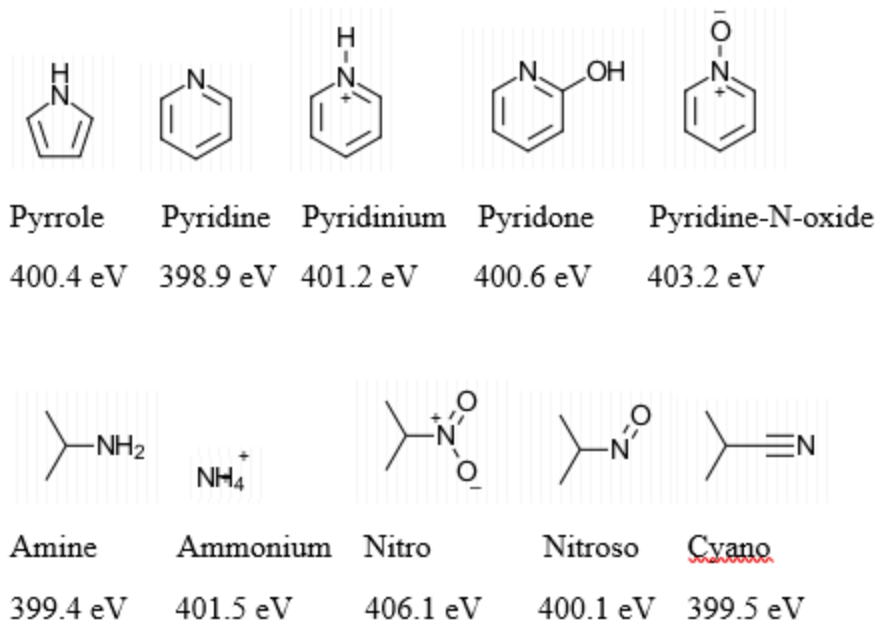
Figure 1-7: Additional bonding patterns for nitrogen in CNx films.

1.2 Motivation

Despite recent advancements to try and replace the current commercially available solar cells, the designs have failed to meet the criteria of being cheap, efficient, and stable for long periods of time. The materials used are often toxic and relatively scarce, which further hinders the goal of being widely implemented. The recent research includes investigation into quantum dot, dye sensitized, organic, and perovskite based solar cells. Carbonaceous materials are stable, abundant, cheap, generally non-toxic, and usually absorb light in the visible and near-infrared regions. All these attributes are beneficial for cheap, efficient, and long lasting solar cells. Carbon nanotubes, graphene and graphene oxide, and fullerenes have been used for various functions in solar cells. Graphene oxide and carbon nanotubes were implemented into organic and dye-sensitized solar cells to act as interfacial layers and electrocatalytic counter electrodes [28 - 32]. There has also been work done on different mixes of carbon nanotubes, graphene oxide, and fullerenes to try and realize all carbon photovoltaic materials [33 – 35]. Graphene sheets have been shown to exhibit carrier photogeneration, but with no emergence of a photovoltaic effect [36].

There are also many different types of carbon nitride films that have been researched over the past few decades. These vary widely in their properties due to the different preparation methods and the large number of different possible bonding configurations in carbon nitride. A lot of the work has been done on films with low nitrogen content [37, 38] as well as graphitic carbon nitride (g-C_3N_4) prepared by chemical synthesis. Both have shown interesting and promising applications, with g-C_3N_4 being heavily researched in the past few years. Its applications include acting as a catalyst for organic reactions [39 - 41], for water splitting [42, 43], and as a material in photochemistry and electrochemistry [44 - 47]. In our group, we have been researching another type of carbon nitride material, high nitrogen content CNx deposited by a radiofrequency magnetron sputtering deposition technique [6, 10]. However, until recently, these materials were only shown to be photoconductive without a true photovoltaic effect. However, it was found that they could be turned into photovoltaic materials by ageing or thermal treatment (annealing). Despite their low efficiencies, the low cost, stability, and low toxicity of these materials provides motivation to explore them further. The application of this material in solar cells is also in its infancy, leaving room for improvement with continued research.

The aim of this thesis was to investigate in detail the properties of high nitrogen content amorphous carbon nitride films (CNx) prepared by a radio frequency (r.f) reactive magnetron sputtering deposition process for application as a semiconductor in solar cells. Specifically, we aimed to reveal the origin of structural changes that were responsible for the switch from photoconductive to photovoltaic behaviour. Also, to develop an optimum carbon nitride film, the deposition procedure had to be researched extensively. Initial properties of high nitrogen CNx films were determined under constant deposition parameters. However, high nitrogen content CNx film properties are highly dependent on the deposition parameters used [18, 23, 48 - 49]. To effectively study the CNx films and the emergence of the photovoltaic behaviour, the effect of the deposition parameters had to be established.

Chapter 2: Experimental

2.1 Preparation and Cleaning of ITO/FTO/Borosilicate Glass

ITO glass was purchased from Delta technologies (R_s = 8-12 Ω, thickness = 0.7 mm), and was cut into 20 mm x 6 mm rectangular pieces. To prevent short-circuiting of the cells, an area of 4 mm x 6 mm at one end of the conductive side of the ITO glass was sanded with a DREMEL 3000 variable-speed rotary tool with a 932 grinding attachment to remove the conducting ITO layer.

FTO glass was purchased from Xin Yan Technology Limited (R_s = 9-11 Ω, thickness = 1.1 mm). and was cut into 20 mm x 6 mm rectangular pieces. A groove was etched into the conductive side of the FTO glass across the width around 6 mm from one of the ends of the glass using a DREMEL 3000 variable-speed rotary tool with a 420 Heavy Duty Cut-off Wheel attachment. The FTO glass was sanded all around the edges using a DREMEL 3000 variable-speed rotary tool with a 932 grinding attachment.

Borosilicate glass was purchased from Coresix (thickness 0.7 mm) and was cut into 20 mm x 6 mm rectangular pieces. No other treatment was performed on the glass before the cleaning steps.

The ITO, FTO and borosilicate glass that were used in all the experiments were cleaned in the same way. They were sonicated in detergent and ~20 mL of milliQ water, followed by 20 mL of acetone, and finally in 20 mL ethanol for 15 minutes each. The ITO and FTO glass were dried with argon gas before being put in an oven for 25 minutes at 90 °C. They were secured onto the substrate holder with double sided carbon tape and transferred into a glovebox. The final step before deposition was securing the substrate holder in the vacuum deposition chamber.

2.2 Deposition of CNx and Aluminum

The process of deposition was the same for all three substrates: ITO, FTO and plain borosilicate glass. A custom-built vacuum deposition system was used that employed a radio frequency magnetron sputtering technique for both carbon (Goodfellow, 99.997 % purity) and aluminum (Kurt J. Lesker, 99.9995 % purity) targets. The holders with the substrates were mounted into the deposition chamber and sealed shut. The distance from the holder to either target

was set at a position of 7 cm. The bias applied to the target varied from 100 - 200 V, depending on the composition of the gases in the chamber. The deposition chamber pressure was brought down to $2x10^{-6} torr$ before a chamber clean was conducted with the corresponding target that was to be used for the deposition. The chamber pressure was then brought down further to $9x10^{-7} torr$ before deposition took place.

For the Schottky cells, the magnetron power was set at 25 W for all depositions, with a chamber pressure of 3 Pa. The CNx depositions used 100 % nitrogen, and varied between 30 and 40 minutes. The aluminum depositions used 100 % aluminum target, and lasted between 20 and 30 minutes. The CNx film was deposited on around a third of the piece of glass. The aluminum film was completely over around half of the CNx film and then a keyhole shape of aluminum was deposited over the other half of the CNx film.

For the CNx films deposited on plain borosilicate glass, the magnetron power was either 25 or 50 W, the chamber pressure either 1,3,5 or 7 Pa, and the % N_2 in the chamber either 25, 75 or 100 %. All depositions were 50 minutes long and the CNx film was deposited on around two thirds of the piece of glass.

2.3 Thermal Annealing of Samples

In some experiments, the samples were annealed after deposition at temperatures between 150 and 350°C for a time between 1 and 2 hours. A custom-built oven was in the glovebox so that the samples were not exposed to atmospheric conditions. The oven had heating elements below and above the samples to ensure uniform heating. The samples were cooled for at least 24 hours before characterization.

2.4 Characterization of the CNx Films

After thermal annealing, the cells were loaded into a custom-built cell holder inside the glovebox. This holder was then taken outside of the glovebox and purged with argon before any measurements were taken. Gold electrodes were connected to either side of the cells inside of the holder. The working electrode was hooked up via an external circuit to the plain, conductive side

of the ITO/FTO glass. The counter electrode was hooked up via an external circuit to the aluminum side of the FTO glass, with the reference electrode connected to the counter electrode wire. A potentiostat/galvanostat model 263A from Princeton Applied Research was used for open circuit, current-voltage, and potentiostatic measurements. The light source used was a 405 nm, 20 mW laser diode from Power Technology which had a light intensity of 2×10^{17} photons s^{-1} cm^{-2}. A 1540XB FIB/SEM machine located in the Western Nanofabrication Facility was used to provide SEM and EDX data. For the UV-Vis data, the samples were clamped in place and were situated in between an incoming light and an outgoing detector. A EPP2000 spectrophotometer from StellarNet was used as the light source and the detector.

2.5 XPS Analysis of CNx Films on Plain Glass

XPS analyses were carried out at Surface Science Western using a Kratos AXIS Nova or Ultra spectrometer, both giving effectively identical results. The X-ray source was monochromatic Al Kα radiation (1486.6 eV). The survey scans were conducted with a pass energy of 160 eV, while the high-resolution scans were recorded with a pass energy of 20 eV. The spot size was 300 x 700 microns, and the photoelectron take-off angle was 90° with respect to the CN$_x$ surface. Each spectrum was background corrected using the Shirley's method. All the binding energies were charge corrected by setting the carbon graphitic peak binding energy to 284.5 eV.

Chapter 3: Properties of High Nitrogen Content CNx Films

3.1 Absorption Coefficients and Spectrum

As discussed previously, CNx must have a suitable absorption spectrum that matches with the solar emission spectrum. As shown in Figure 3-1, there is broad absorption in the visible spectrum, as well as a substantial area in the infrared spectrum. Another advantage is the absorption coefficient of CNx, which was found to be $1.19 * 10^5 nm^{-1}$ from previous research conducted in our group [49]. This is an order of magnitude better than the current silicon solar cells, which are on the order of $10^4 nm^{-1}$ [50]. A favourable absorption band and coefficient means that CNx is a suitable light absorber for solar cells.
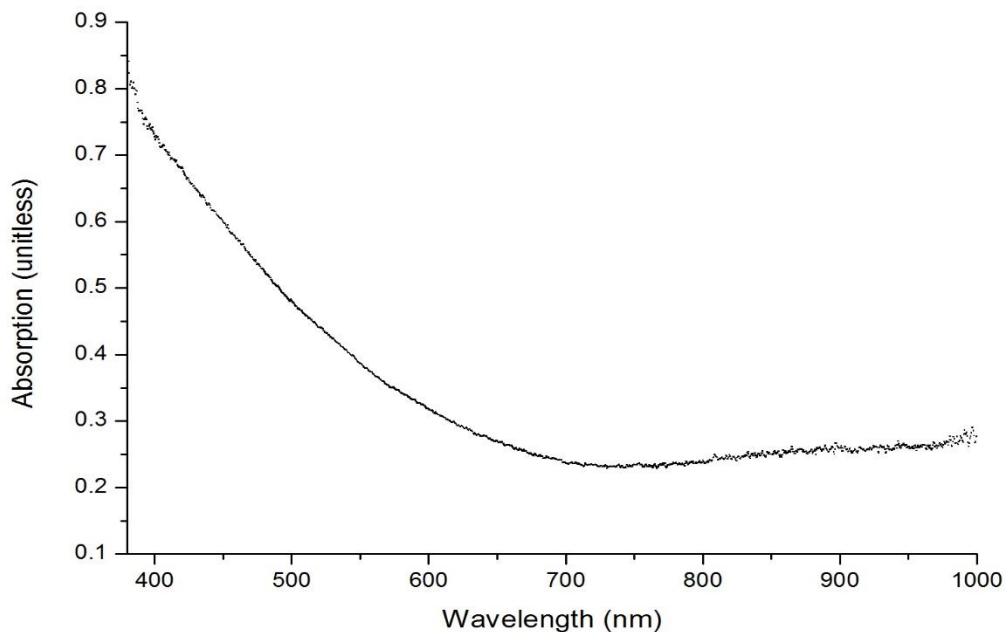
Figure 3-1: Typical absorption band of a CNx film.

3.2 Thickness of CNx Films

UV-Vis spectrophotometry was used on samples with increasing % N$_2$, with all other parameters held constant. The thicknesses of the samples were calculated taking the average of the transmittance values at 405 nm, and using the equation:

$$Thickness = \frac{-\ln(T)}{\alpha}$$

(5)

Where $\alpha = 1.19 * 10^5 nm^{-1}$ at 405 nm. The UV-VIS data is summarized in Table 3-1:

Table 3-1: UV-VIS data for the 4 different % N_2 samples, along with the calculated thicknesses associated with the average transmittance values.

% N_2	Avg. Trans. at 405 nm	Calculated CNx Thickness (nm)
25	0.258	114
50	0.2001	135
75	0.153	158
100	0.156	156

As mentioned previously, the CNx thicknesses tend to plateau at around 75% N_2, which is demonstrated by the almost identical calculated thicknesses for the samples produced using 75% N_2 and 100% N_2. This can be seen visually in Figure 3-2.
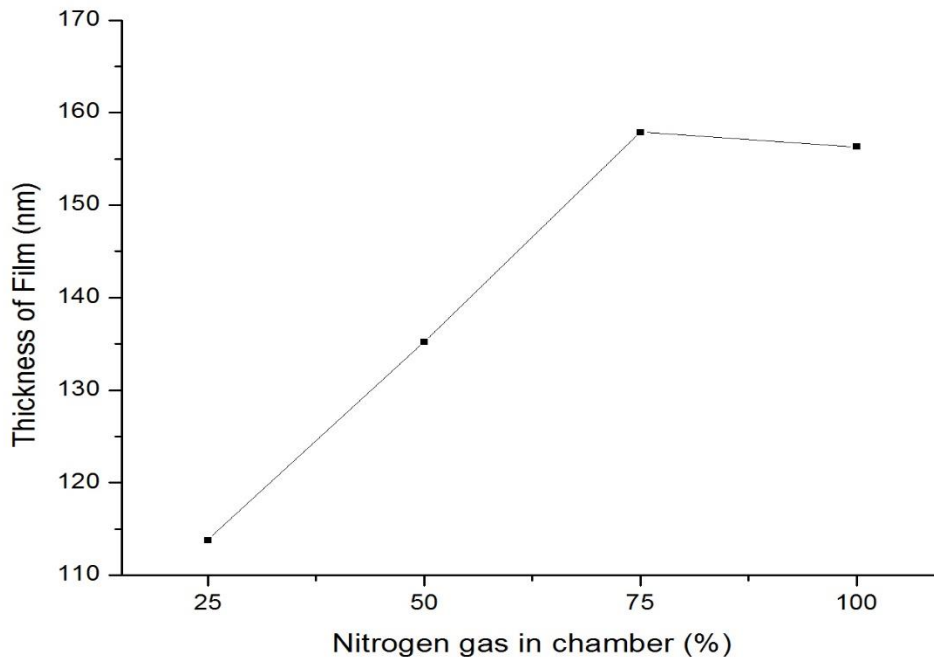
Figure 3-2: Thickness of the CNx layer plotted versus the % of N_2 gas. The samples were all prepared at 50 W and 1 Pa with a deposition time of 40 min.

The reason behind the plateau of the CNx thickness remains unclear and is probably related to the change in the kinetics of film formation, which becomes independent of the nitrogen concentration in the plasma. This is also suggested by our XPS measurements described below. The bonding configurations are also different for different nitrogen percentages as used, as will be discussed later.

3.3 Band Gap of CNx Films

It is possible to use UV-Vis data to estimate the band-gap of an amorphous semiconductor. Tauc plots are employed which plot $(\alpha h v)^{\frac{1}{2}}$ against hv, the photon energy [51]. The linear region of these plots is used to extrapolate to the x axis, which gives an estimate of the material's band-gap, as shown in Figure 3-3 and equation (6):
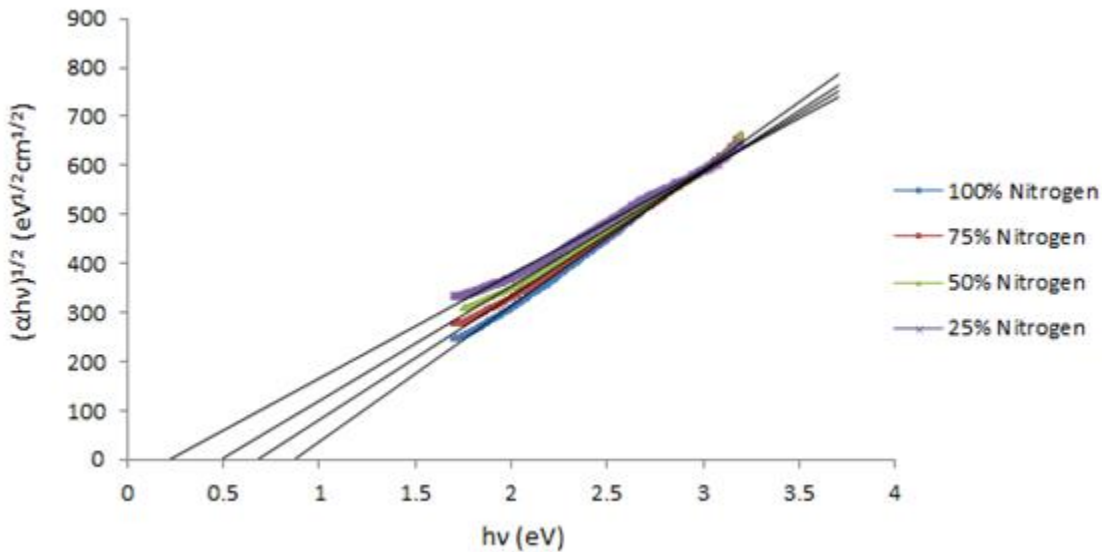
Figure 3-3: Tauc Plots for 25% N₂ (purple), 50% N₂ (green), 75% N₂ (red), and 100% N₂ (blue). The samples were all prepared at 50 W and 1 Pa with a deposition time of 40 min.

$$v^2\alpha \approx \left(hv - E_g\right)^2 \tag{6}$$

The extrapolated lines were used to calculate the band-gap for the four different samples, as summarized in Table 3-2:

Table 3-2: E_{Tauc} values calculated from the lines of best fit from Figure 3-3.

% N_2	Calculated E_{Tauc}(eV)
25	0.217
50	0.495
75	0.676
100	0.869

The calculated E_{Tauc} is shown to clearly increase with increasing % N_2. This matches with previous work done in our group [10]. This may be related to changes in the nitrogen content with increasing % N_2 in the chamber or changes in the bonding pattern. In any case, the band gap increases reaching values close to optimal at high nitrogen contents. This is an important result which emphasizes the importance of increasing the nitrogen content in the film if they are to have applications in solar cells. The solar spectrum has photons with energies ranging from 1.2 – 3.3 eV, so a bandgap just above 1.2 eV is ideal to maintain maximum photovoltage while ensuring that all the incoming photons have enough energy to excite the electrons in the active material.

3.4 Preparation of ITO/FTO-CNx-Al Schottky Cells

The deposition times, powers, pressures, and % N_2 were the same for both the ITO-CNx-Al and the FTO-CNx-Al cells, except for the aluminum deposition times. The deposition time for the cells was 40 minutes for CNx films to prepare a relatively thick layer. The aluminum depositions used for the Schottky cells were 30 minutes for the ITO based cells. This reduced time was to prevent the aluminum from penetrating through the CNx layer and coming into contact with the glass substrate, resulting in the cell short circuiting. The aluminum deposition time for the FTO cells was 20 minutes because there was a bigger issue with the cell short circuiting. Although it was explained before that 75% N_2 and 100% N_2 give similar thicknesses of CNx, 100% N_2 gas was used for the preparation of the cells. This is because it was shown to be more effective at breaking up the graphitic pathways in the film, resulting in a conversion of ohmic to semiconducting behaviour [10]. This is desirable for the cells so that the CNx film can act as an n-type semiconductor. This was confirmed by the increase in the bandgap observed by us with an increase

in the N_2 content (see above). The deposition power was held constant at 25 W to give a higher percent of nitrogen in the CNx film. The cells were made at a pressure of 3 Pa and annealed at 150°C for 1 h, unless noted otherwise.

3.5 Characterization of ITO-CNx-Al Schottky Cells

J-V curves were used to characterize the ITO-CNx-Al Schottky cells made. Figure 4-4 shows the curves for a sample that was in the dark and then exposed to light (dark and light curves). The sample had been left to age for 66 days prior to the data being taken because it was shown in previous work in our group that such ageing improves the photovoltaic effect [59]. The black line that is very close to 0 on the x axis is the J-V curve for the sample under dark conditions, with the red line that has a non-zero slope being the sample when exposed to light. The open circuit voltage is shown to be $-0.102\ V$, while the short circuit current is $0.173\ \mu A$. The open circuit voltage was confirmed with separate open circuit-time measurements (not shown here).
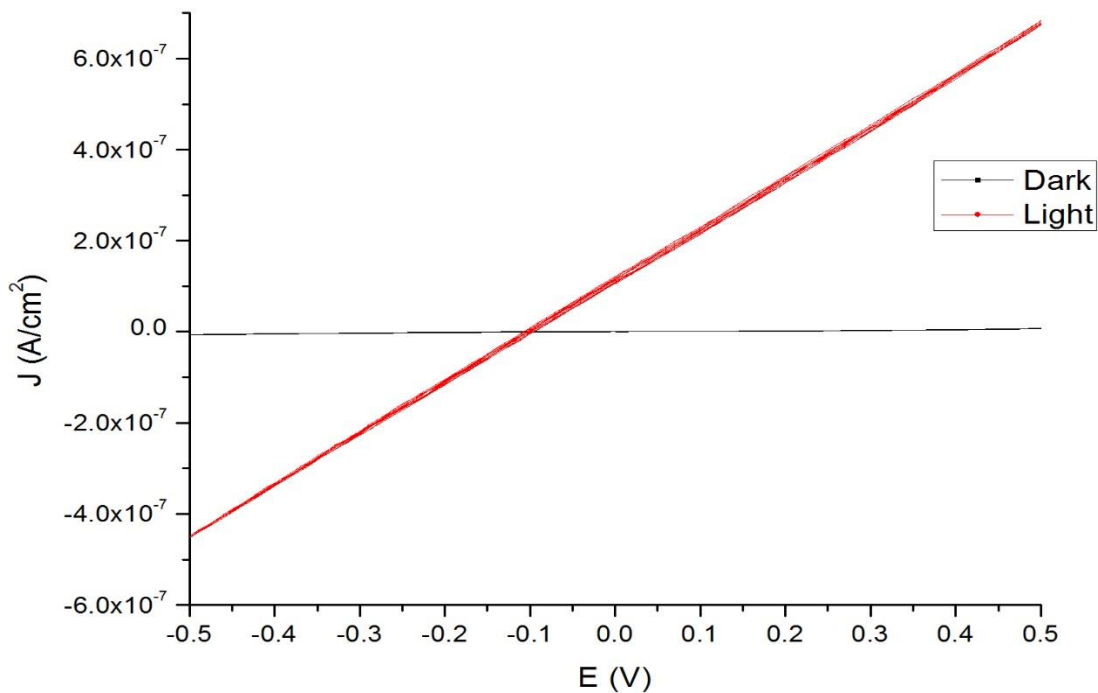
Figure 3-4: J-V Curve of an ITO-CNx-Al cell in the dark (blue) and then exposed to light (orange). The data was taken 66 days after the sample had been made.

Although there is a clear open circuit potential and short circuit current, the linearity of the graph is not desirable since it means a low fill factor. Also, one can see that while there is a negative open-circuit voltage that is consistent with an n-type semiconductor behaviour, the sample demonstrates both anodic and cathodic photocurrents. This means that the CNx in the cell is not an n-type semiconductor, as was expected, and is rather an intrinsic or compensated semiconductor, capable of generating both electrons and holes upon illumination. Ideally the graph would be asymmetrical, non-linear, and have only cathodic photocurrent, which would show that CNx is acting solely as an n-type semiconductor.

Ageing of samples has a profound effect on the quality of the samples. It had been shown that annealing has a similar effect, however we demonstrate here that they have a cumulative effect on the quality of the cells. Table 3-3 shows J-V data of cells taken 3, 42, and 73 days after deposition.

Table 3-3: Comparison between 3 cells aged 3, 42, and 73 days after deposition.

Age of Sample (days after deposition)	Open Circuit Voltage (V)	Short Circuit current (μA)
3	0	0
42	-0.130	0.125
73	-0.156	0.173

All the samples had been annealed at 150 °C for 1 h, and their J-V plots are shown in Figure 3-5. The oldest cell produced the best results, with a V_{OC} of -0.156 V, a I_{SC} of 0.173 μA, a fill factor (FF) of 0.12, and a power conversion efficiency of $3.62 x 10^{-6}$ %. These values are much lower than the averages of 0.5 - 1.5 V for V_{OC}, 0.2 - 80 mA for I_{SC}, 0.4 - 0.6 for FF, and <0.1 % for power conversion efficiency for typical monolayer solar cells [52]. Ageing of the samples still had a clear effect on the samples, with marked improvements in all the cell's parameters. Such an improvement is likely due to film structural relaxation that decreases the degree of compensation and makes the material more of an n-type semiconductor. However, the exact mechanism of the structural relaxation is still unclear. It is possible that the mechanism is like the structural reformation the cell undergoes during thermal annealing. Therefore, annealing at a higher temperature or for a longer time could have a similar effect as letting the cell age for 4 - 8 weeks.

In any case, despite an increase in efficiency, further modifications must be made to the cells for them to be viable for continued research.
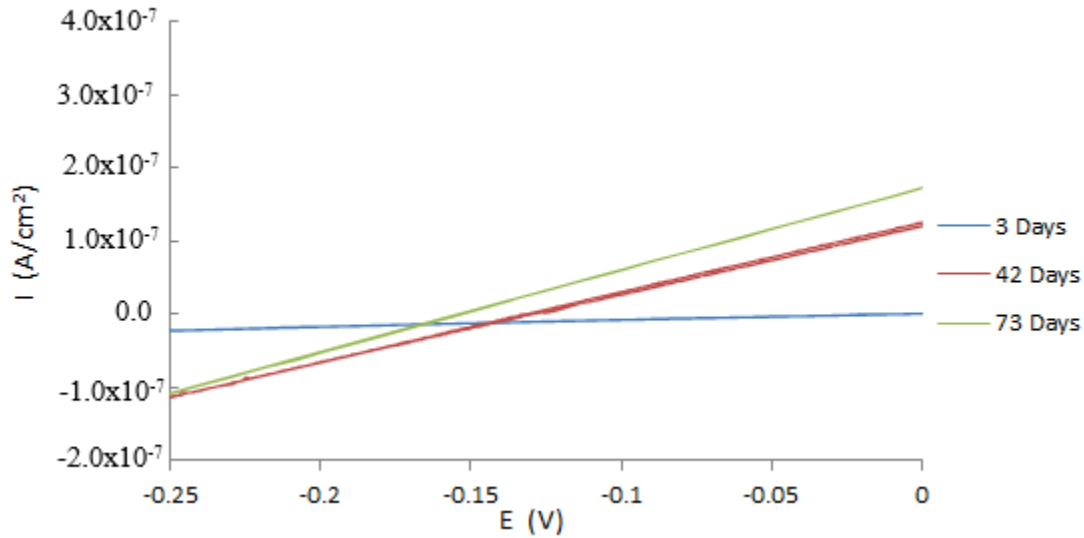
Figure 3-5: J-V Plot of ITO-CNx-Al at 3 (blue), 42 (orange), and 73 (purple) days after deposition.

The formation of a compensated semiconductor has also been demonstrated by time-dependent photocurrent measurements (I-t photocurrent transients). Figure 3-6 shows an I-t graph for a Schottky cell taken 14 days after deposition. The graph shows an initial anodic spike in the photocurrent upon switching the light on, followed by a cathodic spike, before stabilizing on an anodic photocurrent. This cathodic spike demonstrates that the cell is showing p-type characteristics. This means holes are also acting as photogenerated carriers in the cell, resulting in recombination and heavy losses in the cell's photovoltaic properties.
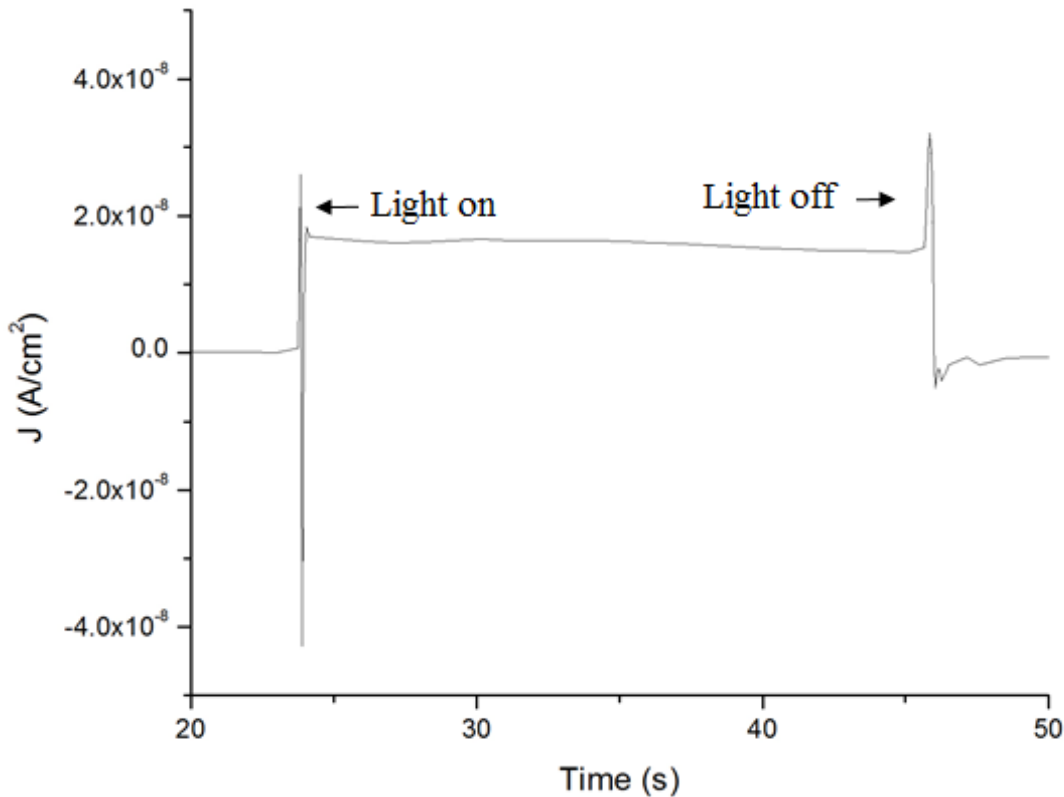
Figure 3-6: I-t graph of an ITO sample taken 14 days after deposition.

3.6 Characterization of FTO-CNx-Al Schottky Cells

FTO glass was substituted for ITO glass to make FTO-CNx-Al Schottky cells. This was done because ITO glass is only stable at temperatures up to ca. 250 °C, while FTO glass has been shown to be stable up to 500 °C. As discussed previously, this could not only circumvent the troublesome practice of waiting 8 weeks for the cells to start showing the photovoltaic properties, it could also alter the cell in more favourable ways. Although the FTO cells made showed higher values for the open circuit voltage than any ITO cells made, the internal/contact resistance in the cells was much too high for them to be viable. In other words, the cells showed photovoltage but too little photocurrent. Figure 3-7 shows the difference in open circuit voltage between a sample that was annealed at 150 °C for 1h, and a sample that was annealed at 150 °C for 2 h. Although the 2 h sample was aged for an extra 7 days, it is much more likely the longer annealing time was the major factor in the much higher open circuit voltage. The lag in the 2 h sample after the light source is turned off is due to the high internal resistance of the cell. It is not noticeable for the 1 h sample

because its conductivity is higher. Once the voltage gets significantly higher in the 2 h sample, the resistance the cell encounters as the photo induced charge carriers attempt to travel back through the cell is apparent. The high resistance of the cell caused the J-V plots, as well as the I-t plots of these samples, to contain too much noise and therefore are not useful to discuss.
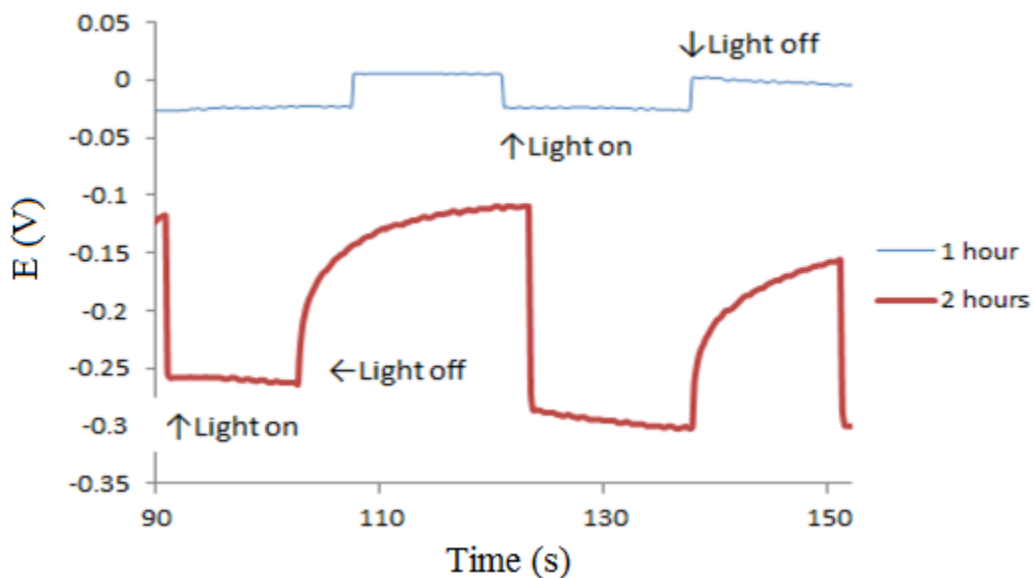
Figure 3-7: Open circuit Vs. time of an FTO-CNx-Al cell in the dark and then exposed to light. Both samples were annealed at 150 °C, one for 1 h (blue), and the other for 2 h (red).

Our data demonstrates that CNx once again forms a compensated semiconductor. Despite its increased open circuit potential, its high resistance and continued compensation of CNx as a semiconductor created an inefficient cell with minimal photovoltaic potential. The next step was to explore the composition and bonding of the films to try and explain the emergence of the photovoltaic effect in the films, as well as how to improve them to make viable solar cells.

Chapter 4: Composition and Bonding of Carbon Nitride Films
4.1 Differences of CNx Films Deposited on ITO and FTO Glass

EDX is a useful technique to confirm the elemental composition of a material. Tables 4-1 and 4-2 outlines the numerical values for both the weight and atomic percent of the main elements (carbon, nitrogen and oxygen) present in CNx samples deposited on ITO and FTO glass, respectively.

Table 4-1: Summary of EDX data for CNx deposited on ITO.

Element	Weight %	Atomic %
C	33.6	38.8
N	30.1	29.8
O	36.2	31.4

Table 4-2: Summary of EDX data for CNx deposited on FTO.

Element	Weight %	Atomic %
C	29.8	34.4
N	14.5	14.8
O	55.7	49.8

The most noticeable difference is the much higher atomic % of oxygen in the FTO sample. Specifically, there is 49.76% oxygen in the FTO cell as compared to 31.39% for the ITO cell. Oxygen could come from a variety of sources, including the carrier gases and trace amounts in the working conditions. When it incorporates into the films, it can either scavenge the extra electrons created by the nitrogen doping, or produce holes due to its unoccupied orbitals. Oxygen has also been shown to induce stress and disorder in the film [53]. An increase in the amount of oxygen in the films grown on FTO as compared to films grown on ITO correlate well with poor photovoltaic effect in those films due to them being compensated semiconductors.

Such a big difference in the semiconductor properties of CNx grown on ITO and FTO substrates was totally unexpected and remains unexplained. One possible hypothesis is the effect of the

substrate morphology. Figures 4-1 and 4-2 show SEM images of CNx deposited on ITO and FTO, respectively. The sample morphology on the ITO is clearly more uniform, with few discernible topographic features. The sample morphology on the FTO is significantly more textured, showing separated mounds of CNx film. The morphological features on the FTO are also much larger in size. The nucleation and growth of CNx films is heavily dependent on the substrate it is deposited onto [54]. It is possible that the differences in morphology in how CNx deposits onto ITO and FTO glass result in more oxygen being incorporated in the CNx film on the FTO cell.
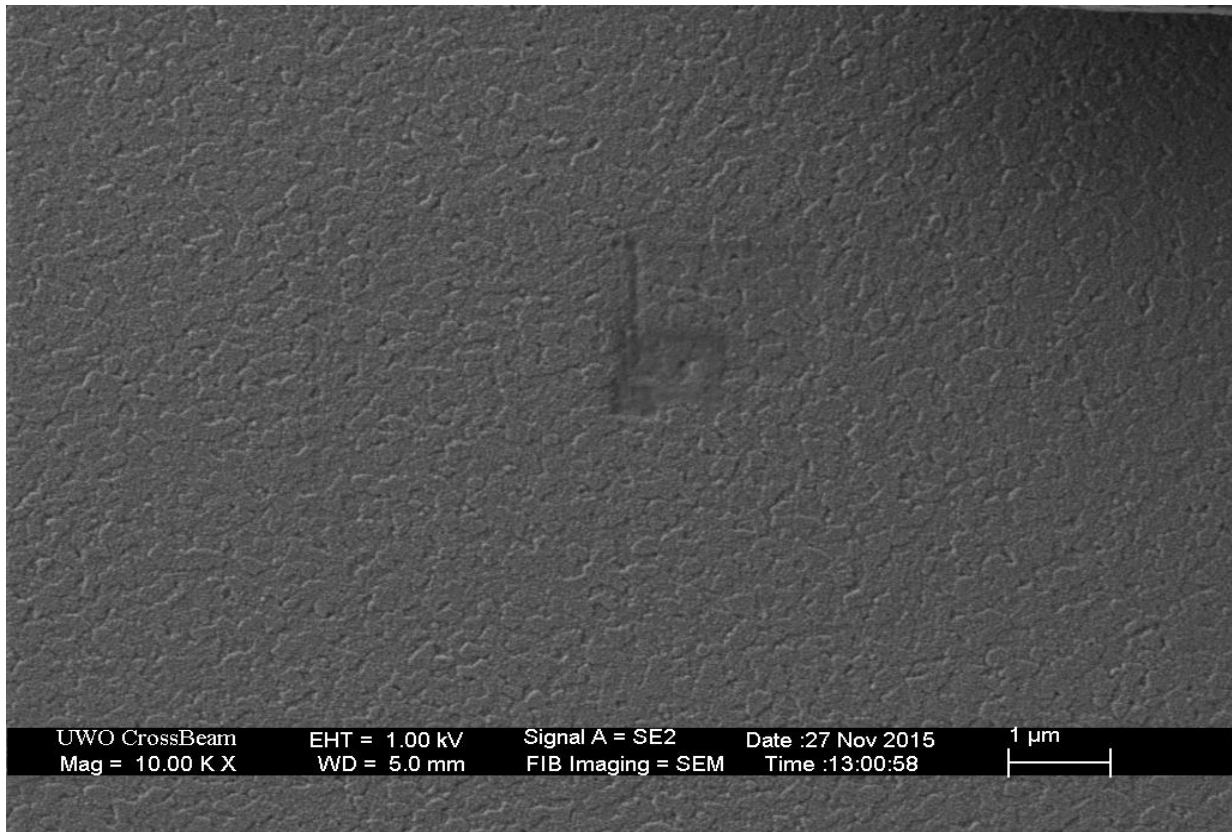
Figure 4-1: SEM image of CNx on ITO glass.
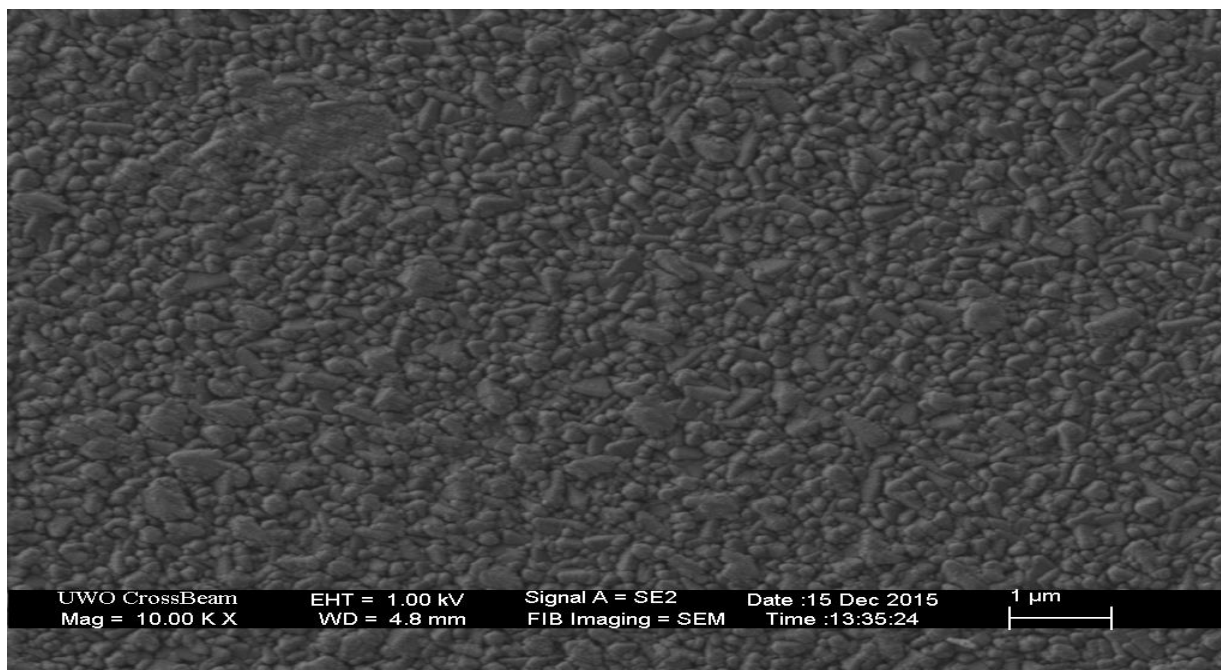
Figure 4-2: SEM image of CNx on FTO glass.

This could help explain the higher resistance found in the FTO cells, where the less uniform morphology helps to impede charge transfer. It is important to note that the differences in morphology may be mainly due to differences in surface texture of the substrates, ITO and FTO. Regardless, it is evident that the final samples have significantly different morphologies which could help explain the differences in the behaviour of cells deposited on ITO as compared to FTO.

4.2 Attempts to Increase Open Circuit Voltage
4.2.1 Different Annealing Environments

Despite the differences in the CNx composition and morphology when deposited on ITO or FTO, there was still the issue of the high oxygen content which remained largely unexplained. The effect of different annealing atmospheres and higher annealing temperatures was explored to eliminate or limit the oxygen content in the deposited CNx films to try and increase the open circuit voltage of the cells. The different annealing atmospheres were pure nitrogen, pure hydrogen, and a 3% hydrogen mixture balanced by argon. The reason eliminating the oxygen was important was because it appeared to be causing CNx to act as a compensated semiconductor, as opposed to the n-type semiconductor that is required for a working photovoltaic device. In addition, annealing

appeared to induce a structural relaxation in the CNx film that could cause it to show better photovoltaic properties. An annealing atmosphere of pure nitrogen was initially chosen, with annealing temperatures of 150ºC and 300ºC for CNx deposited on ITO and FTO glass. The elemental compositions of the CNx films as determined from EDX are shown in Table 4-3 and Table 4-4.

Table 4-3: Elemental composition of a CNx film on ITO glass.

Element	Atomic % (Fresh Sample)	Atomic % (Annealed at 150°C for 1 hour)	Atomic % (Annealed at 300°C for 1 hour)
C	45.2	40.9	38.7
N	34.4	34.8	18.8
O	21.4	24.2	42.5

Table 4-4: Elemental composition of a CNx film on FTO glass.

Element	Atomic % (Fresh Sample)	Atomic % (Annealed at 150°C for 1 hour)	Atomic % (Annealed at 300°C for 1 hour)
C	35.2	31.7	30.1
N	45.9	42.9	39.1
O	17.9	25.4	30.4

The oxygen content is shown to increase with higher annealing temperatures, which exacerbated the problem of oxygen presence in the samples. Figure 4-3 and Figure 4-4 shows a side by side SEM comparison of the fresh versus the annealed CNx films on ITO and FTO glass, respectively. The morphologies of the annealed samples have less texture and are less defined than the fresh counterparts.
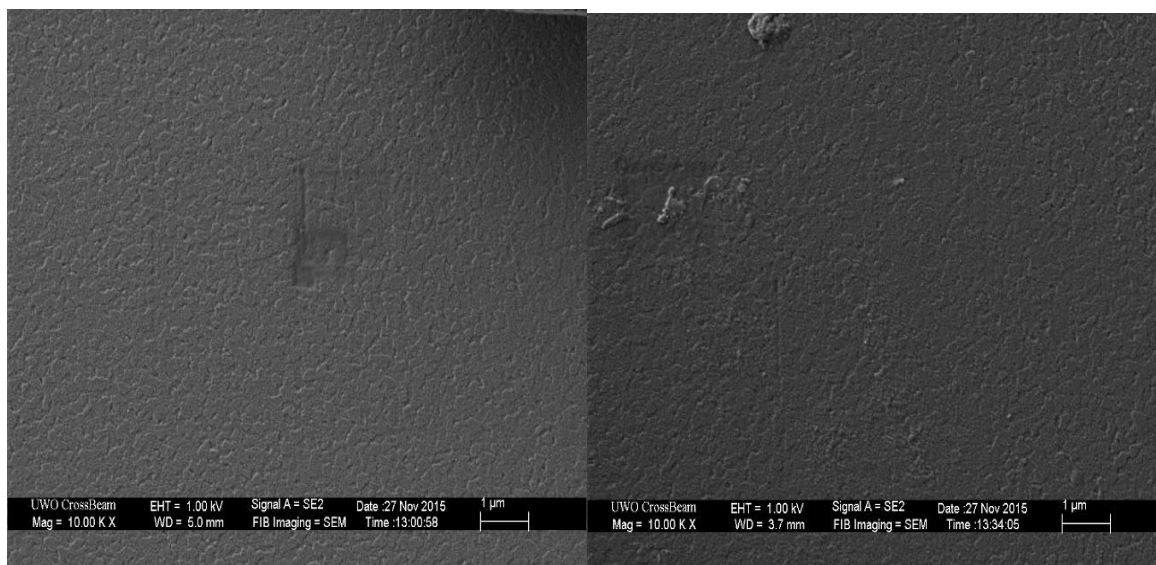
Figure 4-3: SEM image of CNx films on ITO glass, left image is a fresh sample, right image was annealed at 150°C for 1 hour.
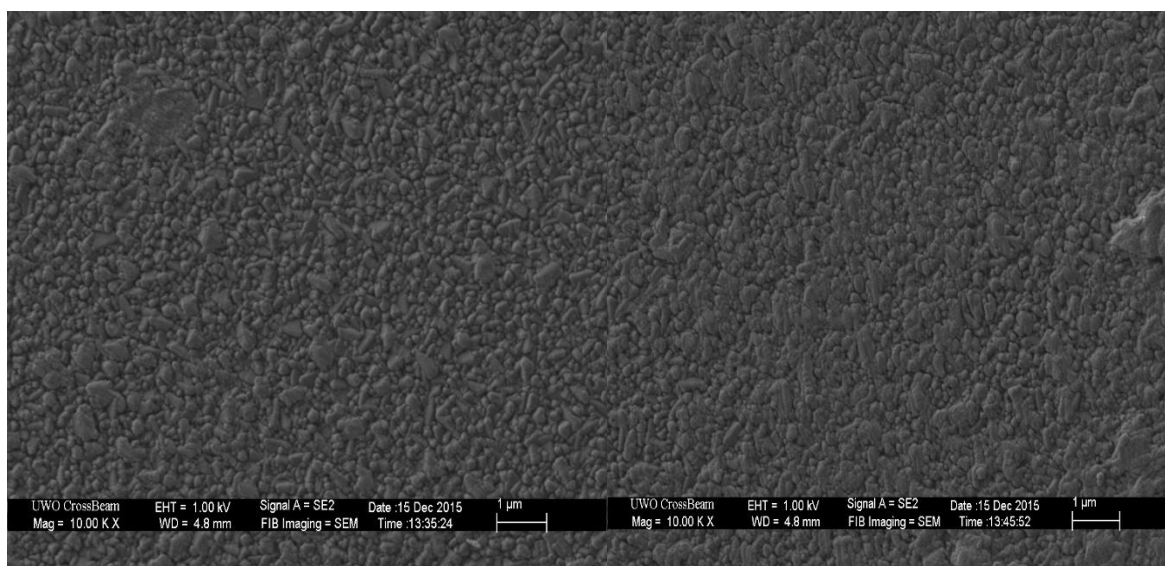
Figure 4-4: SEM image of CNx films on FTO glass, left image is a fresh sample, right image was annealed at 150°C for 1 hour.

Different annealing atmospheres, times, and temperatures were explored to try and eliminate the oxygen content from the films. Higher annealing temperatures and for longer periods of time were designed with the goal that this would result in oxygen evaporating from the samples. Reducing environments with different percentages of hydrogen were also explored to try and encourage the removal of oxygen from the films. The different annealing experiments are summarized in Table 4-5.

Table 4-5: Summary of different annealing experiments performed on CNx films deposited on ITO glass.

Temperature (°C)	Annealing Time (hours)	Annealing Atmosphere
300	2	100% N_2
350	1	100% N_2
150	1	100% H_2
300	1	100% H_2
150	1	3% H_2/97% Ar
150	3	3% H_2/97% Ar

However, these experiments also failed in reducing the oxygen content in the film and it was realized that the oxygen in the FTO and ITO conducting coatings on glass was likely the cause of the oxygen found in the CNx films. At higher annealing temperatures, it is possible the ITO and FTO degraded which would also lead to higher oxygen values. This is more pronounced for ITO as it has a lower thermal stability than FTO. This would explain why the oxygen content was not removed despite the various annealing conditions. Therefore, varying thicknesses of a tungsten film were first deposited on ITO or FTO, followed by CNx. The goal was for the tungsten film to act as a blocking layer to prevent oxygen from transferring from the ITO and FTO into the CNx films. Different annealing experiments were also performed on these cells, as shown in Table 4-6 for ITO based cells and Table 4-7 for FTO based cells.

Table 4-6: Summary of different annealing experiments performed using the ITO-W-CNx architecture.

Temperature (°C)	Annealing Time (hours)	Annealing Atmosphere	Tungsten Thickness (nm)
300	1	100% N_2	2
300	1	100% N_2	3
300	1	100% N_2	4
300	1	3% H_2/97% Ar	4

Table 4-7: Summary of different annealing experiments performed using the FTO-W-CNx architecture.

Temperature (°C)	Annealing Time (hours)	Annealing Atmosphere	Tungsten Thickness (nm)
300	1	100% N_2	2
300	1	100% N_2	3
300	1	100% N_2	4

These experiments still failed to remove the oxygen from the film, with representative elemental compositions of the films shown in Table 4-8.

Table 4-8: Elemental composition of a CNx film deposited on tungsten on FTO glass.

Element	Atomic %
C	40.9
N	34.8
O	24.2

The elemental composition data shows the tungsten did not effectively shield the ITO and FTO layers from the CNx film. Depositing thicker films of tungsten was not an option because the tungsten would block too much light from hitting the CNx film, which would prevent the films from having any application in solar cells. It was decided to remove the FTO/ITO layers altogether, instead opting for plain borosilicate glass with metal deposited straight on it to be used as the electrode.

4.2.1 Different Substrates for CNx Films

There was hesitancy to use metal as the electrode in place of ITO and FTO because you need a thick layer to match the conductivity of ITO/FTO, which lowers the amount of light the CNx receives, which directly affects the power conversion efficiency of the cell. CNx was first deposited only on plain borosilicate glass and the elemental composition was determined using EDX, as shown in Table 4-9.

Table 4-9: Elemental composition of a CNx film deposited on plain borosilicate glass.

Element	Atomic %
C	58.0
N	41.9
O	3.4

A negligible oxygen content was finally achieved for CNx films. Next, silver was tried as the metal contact because it is used in a lot of different solar cell architectures, however it proved to delaminate too easily and was abandoned after the first try. Tungsten was then tried on plain glass which proved to have a much stronger mechanical stability. Table 4-10 show the different annealing experiments that were conducted with the plain glass/tungsten/CNx architecture.

Table 4-10: Summary of different annealing experiments performed using the plain glass-tungsten-CNx architecture.

Temperature (°C)	Annealing Time (hours)	Annealing Atmosphere	Tungsten Thickness (nm)
150	1	100% N_2	4
150	2.5	100% N_2	4
250	1	100% N_2	4

These experiments showed the same negligible oxygen content that was demonstrated with CNx on plain borosilicate glass. This further proves the theory that the oxygen content was arising from the ITO and FTO coating. Table 4-11 shows a representative elemental composition of CNx deposited on tungsten and plain borosilicate glass.

Table 4-11: Elemental composition of a CNx film deposited on tungsten and plain borosilicate glass.

Element	Atomic %
C	56.0
N	40.7
O	3.3

In conclusion, the oxygen from the ITO and FTO coated glass was being incorporated into the CNx films during the deposition procedure. For this reason, different annealing temperatures and conditions were not successful in attempting to remove the oxygen from the films and increase the open circuit voltage. A blocking layer was not able to prevent the leaching of the oxygen from the ITO and FTO coatings. Low oxygen CNx films were created from deposition on plain glass and plain glass with a thin tungsten film.

4.3 XPS Analysis on CNx Films Prepared at Varying Deposition Parameters

Once low oxygen content CNx films were made, further details about the composition and bonding was explored using XPS. The samples were prepared at different deposition powers, % N_2 in the deposition chamber, deposition pressures, and some were annealed at 150°C for 1 hour. The main parameters being explored was the effect of annealing and pressure on the bonding in the CNx films. Three different values for the % N_2 (25, 75 and 100 %), two different values for the deposition power (25 and 50 W) and four different values for the deposition pressure (1,3,5 and 7 Pa) were explored. Table 4-12 summarizes the 24 samples made that were under study in this section. They are split up into four series, which vary in their deposition powers and % N_2 in the deposition chamber, and all include deposition pressures of 1,3,5 and 7 Pa. The starred sample numbers are the annealed samples for visual convenience.

Table 4-12: Deposition parameters used for the 24 samples analyzed.

Series #	Sample ID	%N$_2$ gas in chamber	Deposition Power (W)	Deposition Pressure (Pa)	Annealed at 150°C for 1 hour?
1	D1	100	25	1	No
	D2*	100	25	1	Yes
	D3	100	25	3	No
	D5	100	25	5	No
	D6*	100	25	5	Yes
	D7	100	25	7	No
2	D9	100	50	1	No
	D10*	100	50	1	Yes
	D11	100	50	3	No
	D13	100	50	5	No
	D14*	100	50	5	Yes
	D15	100	50	7	No
3	D19	75	25	1	No
	D20*	75	25	1	Yes
	D21	75	25	3	No
	D23	75	25	5	No
	D24*	75	25	5	Yes
	D25	75	25	7	No
4	D26	25	25	1	No
	D27*	25	25	1	Yes
	D28	25	25	3	No
	D30	25	25	5	No
	D31*	25	25	5	Yes
	D32	25	25	7	No

4.3.1 Analysis of Elemental Composition in CNx Films Determined by XPS

Table 4-13 outlines the elemental compositions determined by XPS of the 24 samples prepared.

Table 4-13: Elemental compositions of the 24 samples determined by XPS.

Series #	Sample	O (%)	N (%)	C (%)	$\frac{N}{C+N}$
1	D1	5.3	37.7	56.1	0.396
	D2*	6.7	34.7	58.6	0.372
	D3	6.9	35.2	56.5	0.384
	D5	7.4	35.8	55.1	0.394
	D6*	9.6	30.1	59.2	0.337
	D7	6.5	36.2	57.1	0.388
2	D9	5.0	33.9	61.1	0.357
	D10*	6.8	33.2	60.0	0.356
	D11	5.6	34.2	60.2	0.363
	D13	8.1	32.5	59.4	0.353
	D14*	9.4	31.5	59.1	0.348
	D15	6.5	34.2	59.3	0.365
3	D19	5.4	34.0	60.6	0.359
	D20*	5.7	34.1	60.2	0.361
	D21	7.5	34.2	58.4	0.369
	D23	7.6	33.7	58.7	0.365
	D24*	7.5	32.7	59.8	0.354
	D25	8.2	34.1	57.7	0.371
4	D26	4.6	34.2	61.2	0.359
	D27*	4.9	34.0	61.2	0.357
	D28	6.7	36.1	57.2	0.387
	D30	6.9	35.5	57.6	0.381
	D31*	6.4	35.9	57.7	0.384
	D32	6.6	36.6	56.7	0.393

The results show that, surprisingly, there is no clear-cut dependence of the nitrogen content in the film on the nitrogen content in the plasma. While the nitrogen content in the plasma was changed from 75% to 25%, the nitrogen content in the film barely changed and stayed just below 40% with some variations that did not show any specific trend. This should indicate that the concentration of nitrogen species in the plasma does not affect the rate of the rate-determining step of CNx formation. It should be noted, however, that all experiments in this chapter were performed at quite low deposition powers of 25 and 50 W. It is possible that the rate of ionization of the carbon target and thus the concentration of carbon containing species in plasma were quite low and thus nitrogen containing species were in relative abundance. Further experiments are needed to clarify this behavior.

4.3.1.1 Effect of Annealing on Elemental Composition in CNx Films

Table 4-14 shows that the nitrogen content in the films either remain constant or lower in value upon annealing. This is especially pronounced for samples D1/D2 and D5/D6, which are all made using the same deposition power and % N_2 in the deposition chamber, as shown in Table 4-12. The change in the overall nitrogen content in the film upon annealing indicates that annealing results in certain chemical and structural transformations that involve nitrogen-containing moieties in the film.

Table 4-14: Effect of annealing on nitrogen content in CNx films.

		$\dfrac{N}{(C+N)}$	
Series #	Sample	Fresh	Annealed
1	D1/D2*	0.396	0.372
	D5/D6*	0.394	0.337
2	D9/D10*	0.357	0.356
	D13/D14*	0.353	0.348
3	D19/D20*	0.359	0.361
	D23/D24*	0.365	0.354
4	D26/D27*	0.359	0.357
	D30/D31*	0.381	0.384

4.3.1.2 Effect of Deposition Parameters on Elemental Composition in CNx Films

There does not appear to be a clear correlation between chamber pressure and nitrogen content. One can speculate that the nitrogen content could slightly increase with pressure; however, the statistical significance of this effect was not demonstrated. The relative nitrogen content for the different samples is outlined in Table 4-15.

Table 4-15: Effect of deposition parameters on nitrogen content in CNx films.

Series #	Deposition Parameters		$\dfrac{N}{(C+N)}$			
	Power (W)	N$_2$ (%)	1 Pa	3 Pa	5 Pa	7 Pa
1	50	100	0.357	0.363	0.353	0.365
2	25	100	0.395	0.395	0.394	0.388
3	25	75	0.359	0.369	0.365	0.371
4	25	25	0.359	0.387	0.381	0.393

4.3.2 Analysis of Nitrogen Bonding in CNx Films Determined by N 1s XPS

It is important to investigate the underlining mechanism for the emergence of the photovoltaic effect within the carbon nitride films. This will allow optimization of the films to try and create solar cells with acceptable efficiencies. To this effect, we studied the effect of annealing, as well as the deposition conditions in general, on the nitrogen bonding patterns in CNx films. As has been already noted, the main nitrogen bonding patterns are pyridinic, pyrrolic and quaternary nitrogen. They differ in their binding energies and thus can be distinguished in N1s high resolution spectra (Fig. 4.5). Quaternary nitrogen represents nitrogen incorporated into graphitic conducting sheets and is an n-doping configuration, whereas pyridinic and pyrrolic moieties are non-doping and furthermore they result in partial break-up of graphitic sheets. Pyridinic nitrogens represent nitrogen that is located at the edges or defects of the graphitic sheets and is essentially indicative of dislocation-like linear defects in graphitic planar sheets formed by graphitic carbon and quaternary nitrogen. Therefore, a decrease in the amount of quaternary nitrogen together with an increase in the abundance of pyridinic fragments would indicate break-up of graphitic sheets and formation of many edges and linear defects. These processes should reduce the conjugation

between graphitic fragments and thus result in a decrease in conductivity and opening of a bandgap.

Therefore, the abundance of the pyridinic structures together with a reduction in the amount of quaternary carbon can be associated with the emergence of the photovoltaic effect. Pyridinic structures posses a lone pair that is not part of the aromatic system. This contrasts with pyrrolic structures which require the nitrogen to donate its lone pair to maintain aromaticity, and quaternary structures where the nitrogen does not posses a lone pair. This free lone pair in the pyrrolic structure leads to the π orbitals undergoing a $\pi \rightarrow \pi^*$ transition, which may be the origin of the photovoltaic response. On the contrary, the quaternary structures will increase photoconductivity due to photoexcited electrons being transferred efficiently over the graphitic network.

One can see from the data of Table 4-16, when the carbon nitride films are annealed, there is a clear and pronounced increase in the abundance of pyridinic structures and a decrease in the abundance of quaternary structures. This results in the breaking up of the graphitic network and separation of photoexcited electron-hole pairs, perhaps by a mechanism similarly to that found in donor-acceptor bulk heterojunction solar cells, whereby photoexcited electrons are trapped at the pyridinic moieties thus facilitating charge separation and the photovoltaic effect. Furthermore, breakup of the graphitic network will result in a decrease in the film conductivity, which should also increase open-circuit voltage according to the well-known diode equation, which predicts that the open-circuit voltage should be greatly enhanced with a decrease in the saturation current due to residual conductivity of the semiconductor material.

A representative N 1s XPS spectrum is shown in Figure 4-5. The high-energy peak represents the quaternary bonding, the middle energy peak the pyrrolic bonding, and the low energy peak the pyridinic bonding.
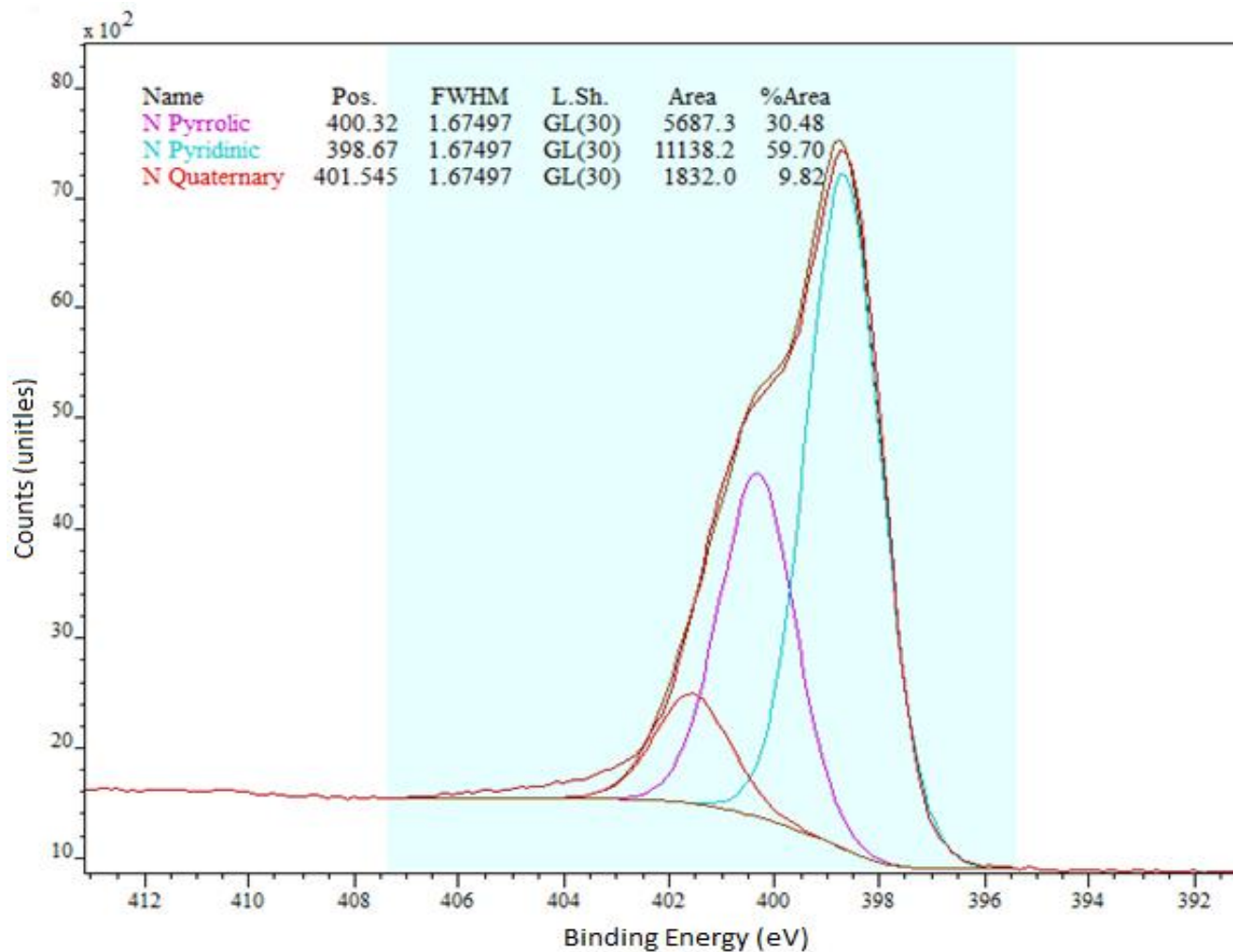
Figure 4-5: Representative N 1s XPS Spectra showing the binding energies for the three different nitrogen bonding configurations.

Table 4-16 outlines the nitrogen bonding percentages determined by XPS of the 24 samples prepared.

Table 4-16: Nitrogen bonding percentages of the 24 samples determined by XPS

Series #	Sample	N Pyridinic	N Pyrrolic	N Quaternary
1	D1	59.7	30.5	9.8
	D2*	49.1	41.0	9.9
	D3	56.6	34.6	8.8
	D5	51.9	33.6	14.5
	D6*	57.5	33.5	9.0
	D7	53.7	32.7	13.6
2	D9	51.4	41.9	6.7
	D10*	63.9	29.4	6.7
	D11	45.4	47.6	7.0
	D13	37.6	51.7	10.7
	D14*	40.5	51.9	7.6
	D15	26.1	66.9	7.0
3	D19	35.2	58.4	6.4
	D20*	35.4	59.2	5.4
	D21	31.0	49.6	19.5
	D23	35.6	51.9	12.5
	D24*	36.3	51.1	12.6
	D25	37.0	49.4	13.7
4	D26	55.6	31.5	12.9
	D27*	60.7	30.4	8.8
	D28	33.1	27.3	39.6
	D30	40.0	41.4	18.5
	D31*	40.6	41.9	17.5
	D32	45.6	32.7	21.7

4.3.2.1 Effect of Annealing on Nitrogen Bonding in CNx Films

The annealed samples in Table 4-17 show a clear increase in nitrogen pyridinic bonding for all samples studied. As discussed previously, this is beneficial for the emergence of the photovoltaic effect. This indicates that annealing is a positive treatment for CNx films for use in solar cells. The increase in pyridinic bonding is more pronounced for the 1st and 2nd series of samples compared to the 3rd and 4th series. This is perhaps due to the lower nitrogen percentage used for the depositions for the 3rd and 4th series.

Table 4-17: Effect of annealing on nitrogen pyridinic bonding in CNx films.

		N Pyridinic Bonding %	
Series #	**Sample**	**Fresh (%)**	**Annealed (%)**
1	D1/D2*	47.1	49.1
	D5/D6*	51.9	57.5
2	D9/D10*	51.4	63.9
	D13/D14*	37.6	40.5
3	D19/D20*	35.2	35.4
	D23/D24*	35.6	36.3
4	D26/D27*	55.6	60.7
	D30/D31*	40.0	40.6

Table 4-18 shows the nitrogen pyrrolic bonding percentages comparing the fresh and annealed samples. There does not appear to be a clear trend for any of the samples, except for a significant decrease for D10 compared to D9 which appears to be an anomaly.

Table 4-18: Effect of annealing on nitrogen pyrrolic bonding in CNx films.

		N Pyrrolic Bonding %	
Series #	Sample	Fresh (%)	Annealed (%)
1	D1/D2*	39.1	41.0
	D5/D6*	33.6	33.5
2	D9/D10*	41.9	29.4
	D13/D14*	51.7	51.9
3	D19/D20*	58.4	59.2
	D23/D24*	51.9	51.1
4	D26/D27*	31.5	30.4
	D30/D31*	41.4	41.9

The annealed samples in Table 4-19 show a clear decrease in nitrogen quaternary bonding for almost all the samples studies. The exceptions are that D10 remains the same as D9, and D24 is negligibly higher than D23. As discussed previously, this is beneficial for the emergence of the photovoltaic effect. This reinforces that annealing is a positive treatment for CNx films for use in solar cells.

Table 4-19: Effect of annealing on nitrogen quaternary bonding in CNx films.

		N Quaternary Bonding %	
Series #	Sample	Fresh (%)	Annealed (%)
1	D1/D2*	13.0	9.9
	D5/D6*	14.5	9.0
2	D9/D10*	6.7	6.7
	D13/D14*	10.7	7.6
3	D19/D20*	6.4	5.4
	D23/D24*	12.5	12.6
4	D26/D27*	13.0	8.9
	D30/D31*	18.5	17.5

Overall, the effect of annealing was shown to increase the pyridinic bonding and decrease the quaternary bonding. It is likely the quaternary bonding configurations were converted to pyridinic moieties during the annealing process, as shown Figure 4-6. The result of this conversion is the break up of the graphitic networks, resulting in less conductive films. It is proposed that this may be cause of the emergence of the photovoltaic effect when samples where annealed.
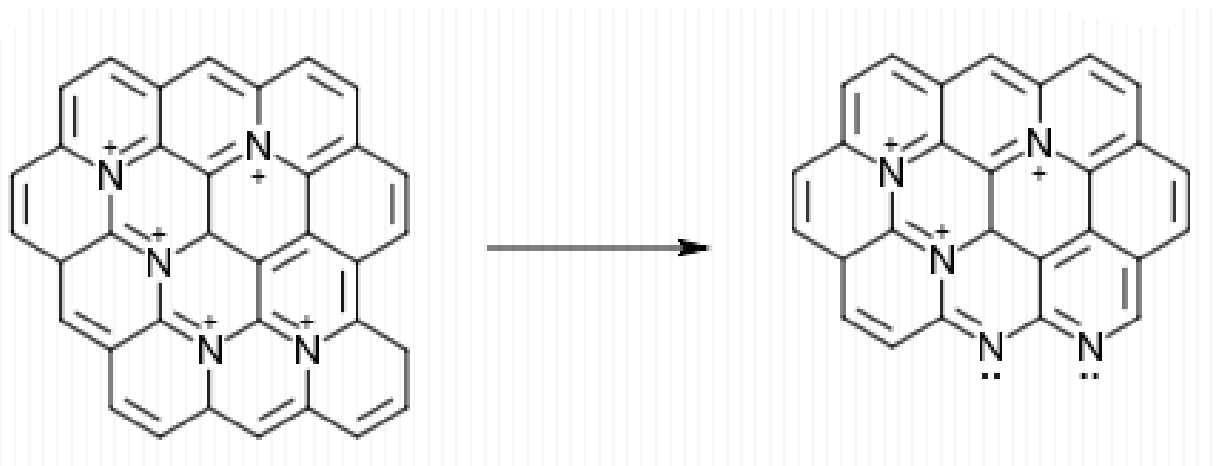
Figure 4-6: Conversion of quaternary nitrogen to pyridinic nitrogen.

4.3.2.2 Effect of Deposition Parameters on Nitrogen Bonding in CNx Films

Table 4-20 shows the nitrogen pyridinic bonding percentages for the prepared samples. For series 1, there is a decrease, while for series 2 and 3 there is a slight increase. The trend for series 4 is not clear. The effect is the most obvious when comparing series 1 and 2 which were prepared at different deposition powers. Series 1 prepared at 50 W experiences a sharp decline in pyridinic bonding with increasing pressure, while series 2 prepared at 25 W slowly increases with increasing pressure. Since pyridinic bonding is generally favoured for photovoltaic performance, higher pressures may be beneficial at 25 W but lower pressures would be better at 50 W. However, increasing pressure always increases the contribution of quaternary nitrogen (see below), which is detrimental for the photovoltaic effect. Therefore, we may conclude that the best chances to make photoactive films are at low deposition powers and pressures and 100% N_2 content in the plasma. This is confirmed by the results of our previous studies [10].

Table 4-20: Effect of deposition parameters on nitrogen pyridinic bonding in CNx films.

Series #	Deposition Parameters		N Pyridinic Bonding %			
	Power (W)	N_2 (%)	1 Pa	3 Pa	5 Pa	7 Pa
1	50	100	51.4	45.4	37.6	26.1
2	25	100	47.1	49.9	51.9	53.7
3	25	75	35.2	31.0	35.6	37.0
4	25	25	55.6	29.2	40.1	45.6

Table 4-21 shows the nitrogen pyrrolic bonding percentages for the prepared samples. Series 1 experiences a sharp increase in pyrrolic bonding with increasing pressure, the opposite effect series 1 demonstrated for pyridinic bonding. At higher pressures and higher deposition powers, pyrrolic nitrogen moieties are favoured over pyridinic ones. There is not any clear pattern for the other series, with series 2 and 4 remaining relatively constant except for an anomaly at 5 Pa for series 4. Series 3 experiences a decline after 1 Pa but then remains effectively constant. Overall, we must conclude that the pyrrolic content fluctuates significantly and does not show any specific trends in our experiments. More data is needed to clarify this behavior.

Table 4-21: Effect of deposition parameters on nitrogen pyrrolic bonding in CNx films.

Series #	Deposition Parameters		N Pyrrolic Bonding %			
	Power (W)	N_2 (%)	1 Pa	3 Pa	5 Pa	7 Pa
1	50	100	41.9	47.6	51.7	66.9
2	25	100	33.2	34.9	33.6	32.7
3	25	75	58.4	49.6	51.9	49.4
4	25	25	31.5	30.8	41.4	32.7

Table 4-22 shows a general increase in nitrogen quaternary bonding with increasing pressure for series 2 – 4. Series 1 remains relatively low when compared with the other series, likely due to the higher deposition power. At the higher deposition power, the nitrogen atoms are less likely to incorporate into the graphitic networks, instead opting to form pyrrolic and pyridinic moieties. All

other series taken at low deposition power clearly show that increasing the pressure favour nitrogen substituting into the graphitic networks in the CNx film.

Table 4-22: Effect of deposition parameters on nitrogen quaternary bonding in CNx films.

Series #	Deposition Parameters		N Quaternary Bonding %			
	Power (W)	N$_2$ (%)	1 Pa	3 Pa	5 Pa	7 Pa
1	50	100	6.7	7.0	10.7	7.0
2	25	100	13.0	11.9	14.5	13.6
3	25	75	6.4	19.5	12.5	13.7
4	25	25	13.0	21.4	18.5	21.7

4.3.3 Analysis of Carbon Bonding in CNx Films Determined by C 1s XPS

The C 1s spectra obtained in this thesis showed multiple peaks, instead of the usual broad, single peak. Similar patterns have been seen in graphitic CNx materials, as well as melamine [55 - 57]. Like these materials, our data shows a low energy peak centered at 248.5 eV which corresponds to carbon bonded to itself in an graphitic configuration. The data was charge corrected by setting this peak to exactly 284.5 eV because it is a well documented binding energy and is clearly separable from the other peaks. The nitrogen content in the CNx films prepared in this thesis are considerably less than for g-C$_3$N$_4$. This results in the higher energy peak being much broader which represents the many different environments nitrogen can participate in. To account for this, the broad peak had to be split up into several peaks to fit the data accurately. A representative C 1s XPS spectrum is shown in Figure 4-7. The two middle peaks are associated with carbon-nitrogen bonding, with the higher energy peak representing carbon single bonded to one nitrogen atom in a pyrrolic fashion (C-N), and the lower energy peak representing carbon double bonded to nitrogen in a pyridinic configuration (C=N) [58]. The low energy peak is our single and double bonded graphitic carbons as discussed above. The highest energy peak, Pi-Pi*, is related to the "shake-up" $\pi - \pi^*$ transition associated with the aromatic carbons. In one sample, D28, there is the appearance of an additional high energy peak attributed to carbon double bonded

to oxygen (C=O) and carbon single bonded to nitrogen with a plus charge (C-N+) [59]. This is unusual because when carbonaceous materials are doped with nitrogen, the carbon-oxygen peaks usually disappear, as demonstrated with the remaining samples prepared [60 - 62].

Name	Pos.	FWHM	L.Sh.		Area	%Area
C=C,C-C	284.5	1.29998	A(0.4,0.38,20)	GL(30)	3369.4	25.98
C Pyrrolic	288.047	1.98643		GL(30)	4364.9	33.65
C Pyridinic	286.536	1.98643		GL(30)	5002.3	38.56
Pi-Pi*	290.912	2.79776		GL(30)	2346	1.81
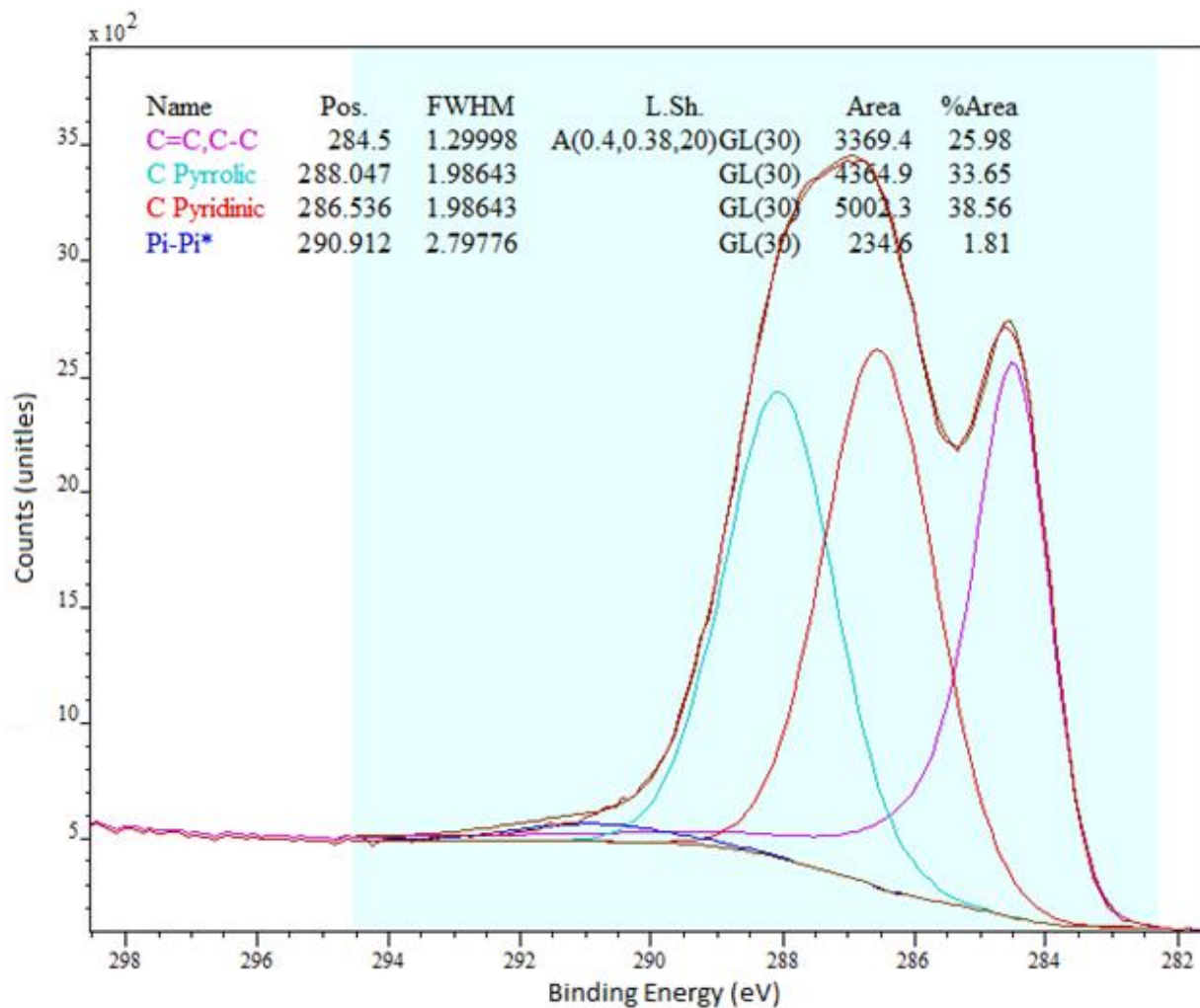
Figure 4-7: Representative C 1s XPS Spectra showing the binding energies for the four different carbon bonding configurations.

Table 4-23 outlines the carbon bonding percentages determined by XPS of the 24 samples prepared.

Table 4-23: Carbon bonding percentages of the 24 samples determined by XPS.

Series #	Sample	C Pyridinic	C Pyrrolic	C Graphitic
1	D1	40.5	33.2	24.6
	D2*	38.1	32.2	27.8
	D3	55.7	34.9	8.8
	D5	38.6	33.6	26.0
	D6*	42.6	29.9	25.7
	D7	38.1	33.9	26.1
2	D9	60.0	25.1	14.0
	D10*	63.4	22.0	12.9
	D11	46.2	28.3	23.9
	D13	44.6	29.8	23.9
	D14*	54.9	26.6	17.3
	D15	41.8	31.3	25.2
3	D19	59.4	27.5	12.2
	D20*	56.5	27.2	15.3
	D21	49.1	38.1	12.0
	D23	42.6	32.8	23.0
	D24*	42.3	33.5	22.6
	D25	38.4	35.8	24.0
4	D26	22.1	60.8	16.0
	D27*	21.4	59.3	18.0
	D28	35.6	42.5	14.9
	D30	39.3	41.1	18.4
	D31*	35.8	38.3	24.3
	D32	39.2	38.0	21.3

4.3.3.1 Effect of Annealing on Carbon Bonding in CNx Films

The annealed samples in Table 4-24 does not show any clear pattern when compared to the fresh samples. This may be because the carbon pyridinic peak also incorporates C=N bonds that are bonded to quaternary nitrogen in the graphitic domains of the CNx film.

Table 4-24: Effect of annealing on carbon pyridinic bonding in CNx films.

Series #	Sample	C Pyridinic Bonding %	
		Fresh (%)	Annealed (%)
1	D1/D2	40.5	38.2
	D5/D6	38.6	42.6
2	D9/D10	60.0	63.5
	D13/D14	44.6	54.9
3	D19/D20	59.4	56.5
	D23/D24	42.6	42.3
4	D26/D27	60.8	59.3
	D30/D31	41.1	38.3

Table 4-25 shows the carbon pyrrolic bonding percentages comparing the fresh and annealed samples. There is a general decrease for the annealed samples, except for the one exception of D24 compared to D23.

Table 4-25: Effect of annealing on carbon pyrrolic bonding in CNx films.

Series #	Sample	C Pyrrolic Bonding %	
		Fresh (%)	Annealed (%)
1	D1/D2	33.2	32.2
	D5/D6	33.7	29.9
2	D9/D10	25.1	22.0
	D13/D14	29.8	26.6
3	D19/D20	27.5	27.2
	D23/D24	32.8	33.5
4	D26/D27	22.1	21.4
	D30/D31	39.3	35.8

Table 4-26 shows the carbon graphitic bonding percentages comparing the fresh and annealed samples. There are slight increases and decreases in percentages but with no clear dependence on the deposition parameters. This shows that annealing involves mostly nitrogen-containing moieties and does not affect purely graphitic fragments in the films.

Table 4-26: Effect of deposition parameters on carbon graphitic bonding in CNx films.

Series #	Sample	C graphitic Bonding %	
		Fresh (%)	Annealed (%)
1	D1/D2	24.6	27.8
	D5/D6	26.0	25.7
2	D9/D10	14.0	12.9
	D13/D14	23.9	17.3
3	D19/D20	12.2	15.3
	D23/D24	23.0	22.6
4	D26/D27	16.0	18.1
	D30/D31	18.4	24.3

4.3.3.2 Effect of Deposition Parameters on Carbon Bonding in CNx Films

Table 4-27 shows the carbon pyridinic bonding percentages for the prepared samples. The bonding percentages decrease with increasing deposition pressure for all the series, which is similar to what was obtained from N1s spectra. As for the dependence on the deposition power and nitrogen content in the plasma, no clear trends can be discerned. This is at variance with the trends observed for nitrogen pyridinic bonding, which provides more evidence that the carbon pyridinic peak also incorporates C=N bonds that are bonded to quaternary nitrogen in the graphitic domains of the CNx film.

Table 4-27: Effect of deposition parameters on carbon pyridinic bonding in CNx films.

Series #	Deposition Parameters		C Pyridinic Bonding %			
	Power (W)	N_2 (%)	1 Pa	3 Pa	5 Pa	7 Pa
1	50	100	60.0	46.2	44.6	41.8
2	25	100	40.5	55.7	38.6	38.1
3	25	75	59.4	49.1	42.6	38.5
4	25	25	60.8	42.5	41.1	38.0

Table 4-28 demonstrates how the carbon pyrrolic bonding percentages generally increase with increasing deposition pressure. The correlation is strongest when comparing samples made at 1 Pa to samples made at higher pressures. When comparing series 2 to series 1, it appears that increasing deposition power results in less carbon pyrrolic bonding. At low pressure, there is also a clear decrease in carbon pyrrolic bonding with decreasing % N_2 in the deposition chamber. The significance of these changes is not entirely clear at the moment.

Table 4-28: Effect of deposition parameters on carbon pyrrolic bonding in CNx films.

Series #	Deposition Parameters		C Pyrrolic Bonding %			
	Power (W)	N_2 (%)	1 Pa	3 Pa	5 Pa	7 Pa
1	50	100	25.1	28.3	29.8	31.3
2	25	100	33.2	34.9	33.7	34.0
3	25	75	27.5	38.1	32.8	35.8
4	25	25	22.1	35.6	39.3	39.3

Table 4-29 shows the carbon graphitic bonding percentages for the prepared samples. There is an increase in the values with increasing pressure for all the series except an anomaly at 3 Pa for series 2. Valuable information can be derived if Table 4-29 is compared to the nitrogen quaternary bonding shown in Table 4-22. Series 1 – 3 demonstrate relatively high carbon graphitic bonding without the accompanying nitrogen quaternary bonding. This demonstrates that there is a significant graphitic network in the CNx films without nitrogen doping occurring, which is detrimental to the emergence of the photovoltaic effect. However, the values for graphitic carbon bonding and nitrogen quaternary bonding for series 4 are similar. This indicates that when low % N_2 is used in the deposition chamber, lots of nitrogen is incorporated into the graphitic networks in the CNx films.

Table 4-29: Effect of deposition parameters on carbon graphitic bonding in CNx films.

Series #	Deposition Parameters		C Graphitic Bonding %			
	Power (W)	N_2 (%)	1 Pa	3 Pa	5 Pa	7 Pa
1	50	100	14.0	23.9	23.9	25.2
2	25	100	24.6	8.8	26.0	26.1
3	25	75	12.2	12.0	23.0	24.0
4	25	25	16.0	14.9	18.4	21.3

4.4 Conclusions

The effects that the different deposition parameters had on the elemental compositions and bonding configurations are summarized in Table 4-30. From this table, it demonstrates that the most pronounced net effect of annealing is to increase nitrogen pyridinic bonding at the expense of nitrogen quaternary bonding, with a negligible effect on the carbon bonding in the film. The effect of the deposition power cannot be clearly established because too few powers were investigated. Increasing the % N_2 in the deposition chamber surprisingly did not result in clear changes in the nitrogen content in the film. At the same time, it increases nitrogen pyridinic bonding at the expense of nitrogen quaternary bonding, and has a negligible effect on the carbon bonding configurations. Increasing the deposition pressure increases nitrogen quaternary bonding while decreasing nitrogen pyridinic bonding, and increases carbon pyrrolic and graphitic bonding which causes carbon pyridinic bonding to decrease.

Table 4-30: Summary of the effects deposition power, pressure, % N_2 in the chamber, and annealing had on the elemental compositions and bonding configurations of the CNx films.

Parameter	Annealing	Higher Power	Higher % N_2	Higher Pressure
Nitrogen Content	No Clear Effect	No Clear Effect	No Clear Effect	No Clear Effect
N Pyridinic Bonding	**Increase**	Decrease	Increase	Decrease
N Pyrrolic Bonding	No Clear Effect	No Clear Effect	No Clear Effect	No Clear Effect
N Quaternary Bonding	**Decrease**	Decrease	Decrease	Increase
C Pyridinic Bonding	No Clear Effect	Increase	Decrease (only at low pressure)	Decrease
C Pyrrolic Bonding	Slight Decrease	Decrease	Decrease (only at low pressure)	Increase
C Graphitic Bonding	No Clear Effect	No Clear Effect	No Clear Effect	Increase

Chapter 5: Conclusions and Future Work

The properties of vacuum deposited CNx thin films were explored for films grown using a variety of substrates, deposition parameters, and various kinds of post-deposition treatments. CN_X films demonstrated a suitable absorption spectrum for application in solar cells, absorbing light across the visible and near-infrared spectrum. UV-Vis spectroscopy showed a linear increase of film thickness from 25% N_2 up until 75% N_2, with the thickness for 100% N_2 being effectively the same as for 75% N_2. Tauc plots were also produced from the UV-Vis data to estimate the band-gap of the CNx films. It was shown that the band-gap slowly increases with increasing %N_2 at the deposition parameters used.

CNx and aluminum were deposited onto ITO glass to form a Schottky cell with an ITO-CNx-Al architecture. The cells showed that they could produce a photocurrent as shown in J-V plots, however the efficiencies of the cells were low. Ageing of the cells in inert conditions significantly improved their performance, most likely due to structural relaxation. However, CNx demonstrated the properties of a compensated semiconductor, indicating both holes and electrons were acting as photogenerated carriers.

CNx and aluminum were also deposited onto FTO glass to form a Schottky cell with an FTO-CNx-Al architecture. The same ageing effect was also demonstrated in FTO cells using J-V plots, however those samples had zero open circuit potential. Annealing different FTO cells for a longer period showed a significant increase in open circuit potential. Despite the FTO cells showing a pronounced increase in open circuit potential, the high resistance in the films prevented the desired results. It was also shown that CNx continued to act as a compensated semiconductor.

SEM data of CNx deposited on ITO and FTO showed significant differences in morphology of the two films, which helped to explain the differences shown between the cell properties. Energy-dispersive X-ray Spectroscopy (EDX) showed a very substantial component of the CNx films was oxygen for both ITO and FTO, although it was more pronounced in the CNx films on FTO. This helped to explain the compensated semiconductor nature of the CNx film in both types of cells.

Due to the negative effect of the high oxygen content in the carbon nitride films on the open circuit voltage, different annealing conditions were implemented to try and eliminate or lower the value of oxygen. Pure nitrogen, pure hydrogen and a 3% hydrogen mixture balanced by argon at different annealing temperatures all failed to remove or lower the oxygen content in the films. It was discovered that the oxygen from the ITO and FTO glass was being incorporated into the CNx films, causing the high oxygen content. Metal blocking layers were unsuccessful in preventing this leaching, so the ITO and FTO glass was replaced with plain borosilicate glass with thin film tungsten replaced the ITO and FTO as the electrode. This was successful in significantly lowering the oxygen content to negligible values in the CNx films.

XPS analysis was carried out on the low oxygen content CNx films to study the effect different deposition parameters had on the properties of the film. It was demonstrated that deposition power, pressure, the % N_2 in the deposition chamber, and post-deposition annealing all had effects on the elemental compositions and bonding configurations within the CNx film. Specifically, the positive effect of annealing on the photovoltaic properties of the films was related to formation of more pyridinic moieties in the CNx films and the associated break-up of the conducting graphitic network, including that doped with quaternary nitrogen.

More work needs to be done to explore the full effects of the deposition parameters on the bonding configurations within the CNx films. Series with a wider range of deposition powers and nitrogen content in the chamber need to be made and analyzed. This will further explain the origin of the photovoltaic effect and determine the optimal deposition parameters for CNx films for applications for solar cells. Once this is established, a transparent conducting glass that would not incorporate oxygen into the CNx films would ideally be found. These would be the first steps towards realizing a solar cell based only on a carbonaceous active material.

References

1. Robertson, J. Materials Science & Engineering R-Reports, **2002**, *37*, 129.

2. Robertson, J.; Oreilly, E.P. Physical Review B, **1987**, *35*, 2946 – 2957.

3. McCreery, R. L. Chemical Reviews, **2008**, *108*, 2646.

4. Lazar, G.; Clin, M.; Charvet, S., Diamond and Related Materials, **2003,** *12*, 201-207.

5. Mckenzie, D. R.; Yin, Y.; Marks, N. A.; Davis, C. A.; Pailthorpe, B. A.; Amaratunga, G. A. J.; Veerasamy, V. S. *Diamond and Related Materials,* **1994**, *3*, 353.

6. Alibart, F.; Durand-Drouhin, O.; Debiemme-Chouvy, C.; Benlahsen, M., *Solid State Communications,* **2008,** *145,* 392-396.

7. Muhl, S.; Rodil S. *Diamond and Related Materials,* **2004,** *13*, 1521 – 1531.

8. Robertson, J.; Davis, C., *Diamond and Related Materials,* **1995,** *4,* 441-444.

9. Sjostrom, H.; Stafstrom, S.; Boman, M.; Sundgren, J. E. *Physical Review Letters,* **1995**, *75*, 1336.

10. Byers, J.C. PhD Dissertation, Western University, **2013.**

11. Mubumbila, N. ; Tessier, P.Y.; Angleraud, B.; Turban, G., *Surface and Coatings Technology,* **2002,** *151-152,* 175-179.

12. Peponas, S.; Benlahsen, M.; Guedda, M., *Journal of Applied Physics,* **2009,** *106.*

13. Alibart, F.; Durand Drouhin, O., *Applied Surface Science,* **2008,** *254,* 5564-5568.

14. Durand-Drouhin, O.; Benlahsen, M. *Solid State Communications,* **2004**, *13*, 425

15. Lejeune, M.; Benlahsen, M., *Diamond and Related Materials,* **2008,** *17,* 29-35.

16. Muhl, S.; Mendez, J. *Diamond and Related Materials,* **1999,** *8*, 1809 - 1830

17. Durand-Drouhin, O.; Lejeune, M.; Clin, M.; Ballutaud, D.; Benlahsen, M. *Solid State Communications,* **2001**, *118*, 179

18. Byers, J.C.; Billon, F.; Debiemme-Chouvy, C.; Deslouis, C.; Pailleret, A.; Semenikhin, O.A. *Acs Applied Materials & Interfaces,* **2012**, *4*, 4579 – 4587.

19. Peponas, S.; Guedda, M.; Benlahsen, M., *Solid State Communciations,* **2008,** *146*, 78-82.

20. Kaltofen, R.; Sebald, T.; Weise, G. *Thin Solid Films,* **1996**, *290*, 112 – 119.

21. Therasse, M.; Benlahsen, M. *Solid State Communications*, **2004**, *129*, 139 – 142.

22. Ronning, C.; Feldermann, H.; Merk, R.; Hofsass, H.; Reinke, P.; Thiele, J. U. *Physical Review B,* **1998**, *58*, 2207 – 2215.

23. Lejeune, M.; Durand-Drouhin, O.; Charvet, S.; Grosman, A.; Ortega, C.; Benlahsen, M. *Thin Solid Films,* **2003***, 444*, 1 – 8.

24. Pels, J. R.; Kapteijn, F.; Moulun, J. A.; Zhu, Q.; Thomas, K. M. *Carbon*, **1995**¸ *33*,   1641 – 1653.

25. Nallathambi, V.; Li, X.; Lee, J.; Popov, B. N. *ESC Transactions*, **2008,** *16*, 405 – 417.

26. Shao, Y.; Zhang, S.; Engelhard, M. H.; Li, G.; Shao, G.; Wang, Y.; Liu, J.; Aksay, I. A.; Lin, Y. *Journal of Materials Chemistry*, **2010**, *20*, 7491-7496.

27. Reddy, A. L. M.; Srivastava, A.; Gowda, S. R.; Gullapalli, H.; Dubey, M.; Ajayan, P. M. *ACS Nano,* **2010**, *4*, 6337 – 6342.

28. He, M.; Jung, J.; Qiu, F.; Lin, Z. *Journal of Material Chemistry*, **2012**, *22*, 24254 – 24264.

29. Zhang, D.W.; Li, X.D.; Li, H.B.; Chen, S.; Sun, Z.; Yin, X.J. *Carbon*, **2011**, *49*, 5382–5388.

30. Yin, Z.; Sun, S.; Salim, T.; Wu, S.; Huang, X.; He, Q. *ACS Nano*, **2010**, *4,* 5263–5268.

31. Salvatierra, R. V.; Cava, C.E.; Roman, L.S.; Zarbin, A.J.G. *Advanced Functional Materials*, **2013**, *23,* 1490–1499.

32. Bernardi, M.; Lohrman, J.; Kumar, P.; Kirkeminde, A.; Ferralis, N. Grossman, J.C. *ACS Nano*, **2012**, *6,* 8896–9903.

33. Tung, V.C.; Huang, J. H.; Kim, J.; Smith, A.J.; Chu, C. W.; Huang, J. *Energy and Environmental Science*, **2012**, *5,* 7810 – 7818.

34. Jain, R.M.; Howden, R.; Tvrdy, K.; Shimizu, S.; Hilmer, A.J.; McNicholas, *Advanced Materials,* **2012**, *24,* 4436–4439.

35. Freitag, M.; Low, T.; Xia, F.; Avouris, P. *Nature Photonics*, **2012**, *7,* 53–59.

36. Lagrini, A.; Charvet, S.; Benlahsen, M,; Debiemme-Chouvy, C.; Deslouis, C.; Cachet, H. *Thin Solid Films*, **2005**, *482,* 41 – 44.

37. Kaltofen, R.; Sebald, T.; Weise, G. *Thin Solid Films*, **1996**, *290*, 112 – 119

38. Su, F.Z.; Mathew, S.C.; Lipner, G.; Fu, X.Z.; Antonietti, M.; Blechert, S. Wang, X.C *Journal of the American Chemical Society*, **2010**, *132,* 16299–16301.

39. Goettmann, F.; Fischer, A.; Antonietti, M.; Thomas, A. *Angewandte Chemie International,* **2006**, *45*, 4467–4471.

40. Chen, X.F.; Zhang, J.S.; Fu, X.Z.; Antonietti, M.; Wang, X.C. *Journal of the American Chemical Society*, **2009**, *131*, 11658–11659.

41. Dong, J.F.; Wang, M.; Li, X.Q.; Chen, L.; He, Y.; Sun, L.C. *ChemSusChem*, **2012**, *5*, 2133–2138.

42. Wang, T.; Di, Y.; Antonietti, M.; Li, H.R.; Chen, X.F.; Wang, X.C. *Chemistry Materials* **2010**, *22*, 5119–5121.

43. Lee, E.Z.; Jun, Y.S.; Hong, W.H. Thomas, A. Jin, M.M. *Angewandte Chemie International,* **2010**, *49*, 9706–9710.

44. Zhang, Y.H.; Pan, Q.W.; Chai, G.Q.; Liang, M.R. Dong, G.P. Zhang, Q.Y. Qiu, J.R. *Scientific Reports*, **2013**, 1943.

45. Reyes, R.; Legnani, C. Ribeiro Pinto, P.M.; Cremona, M. *Applied Physics Letters*, **2003**, *82*, 4017–4019.

46. Iwano, Y.; Kittaka, T.; Tabuchi, H.; Soukawa, M.; Kunitsugu, S.; Takarabe, K. Itoh, K. *Japan Journal of Applied Physics,* **2008**, *12*, 7842–7844.

47. Zhang, Y.J.; Schnepp, Z.; Cao, J.Y.; Ouyang, S.X.; Li, Y.; Ye, J.H.; Liu, S.Q. *Scientific Reports*, **2013**, 2163.

48. Hellgren, N.; Johansson, M. P.; Broitman, E.; Hultman, L.; Sundgren, J. E. *Physical Review B*, **1999**, *59*, 5162 – 5169.

49. Byers, J.C.; Billon, F.; Debiemme-Chouvy, C.; Deslouis, C.; Pailleret, A.; Semenikhin, O.A. *Acs Applied Materials & Interfaces,* **2012**, *4*, 4579

50. Shi, G.; Kioupakis, E. *ACS Photonics*, **2015**, *2*, 208 – 218.

51. Tauc, J.; Grigorov. R; Vancu, A. *Physica Status Solidi,* **1966**, *15*, 627

52. Spanggaard, H.; Krebs, F.C. *Solar Energy Materials and Solar Cells* **2004,** *83*, 125

53. Li, X.; Wang, H.; Robinson, J. T.; Sanchez, H.; Diankov, G.; Dai, H. *Journal of the American Chemical Society*, **2009**, *131*, 15939 – 15944.

54. Byers, J.C.; Tamiasso-Martinhon, P.; Deslouis, C.; Pailleret, A.; Semenikhin, O.A. *Journal of Physical Chemistry,* **2010**, *114*, 18474

55. Wei, D.; Liu, Y.; Wang, Y.; Zhang, H.; Huang, L.; Yu, G. *Nano Letters*, **2009,** *9,* 1752 – 1758.

56. Dementjev, A. P.; de Graaf, A.; van de Sanden, M. C. M.; Maslakov, K. I.; Naumkin, A. V.; Serov, A. A. *Diamond and Related Materials,* **2000**, *9*, 1904 – 1907.

57. Guo, Q. X.; Xie, Y.; Wang, X. J.; Zhang, S. Y.; Hou, T.; Lv, S. C. *Chemical Communications,* **2004**, *1*, 26 - 27.

58. Hellgren, N.; Guo, J. H.; Luo, Y.; Sathe, C.; Agui, A.; Kashtanov, S.; Nordgren, J.; Agren, H.; Sundgren, J. E. *Thin Solid Films* **2005**, *471*, 19.

59. Miller, D. J.; Biesinger, M. C.; McIntyre, N. S. *Surface and Interface Analysis*, **2002**, *33*, 299 – 305.

60. Zhang, C.; Fu, L.; Liu, N.; Liu, M.; Wang, Y.; Liu, Z. *Advanced Materials*, **2011**, *23*, 1020 – 1024.

61. Sheng, Z. H.; Shao, L.; Chen, J. J.; Bao, W. J.; Wang, F. B.; Xia, X. H. *ACS Nano,* **2011**, *5*, 4350 – 4358.

62. Lin, Y. C.; Lin, C. Y.; Chiu, P. W. *Applied Physics Letters*, **2010**, *96*, 133110.

63. Long, D.; Li, W.; Ling, L.; Miyawaki, J.; Mochida, I.; Yoon, S. H. *Langmuir*, **2010**, *26*, 16096 – 16102.

David Pipher

ACADEMIC QUALIFICATIONS

2013 - Present   **University of Western Ontario**
MSc Candidate, 2016
Research area: Physical Chemistry
Concentration: Photovoltaics

2009 - 2013   **McGill University**
Bachelor of Science (Honours)
Major: Chemistry
Concentration: Atmosphere and Environment

TEACHING EXPERIENCE

2016 - Present   **Senior Events Coordinator, Let's Talk Science**
University of Western Ontario, London, Canada
- Coordinate and manage the Let's Talk Science site at Western University

2014 - Present   **Private Tutor for Organic Chemistry**
University of Western Ontario, London, Canada
- Tutoring a variety of students in multiple courses

2015 - 2016   **Community Events Coordinator, Let's Talk Science**
University of Western Ontario, London, Canada
- Coordinate science outreach events across the greater London area

2013 - 2016   **Teaching Assistant for Discovering Chemical Structure and Discovering Chemical Energetics**
University of Western Ontario, London, Canada
- Teaching and supervising labs to class sizes of 20+

VOLUNTEERING EXPERIENCE

2015 - Present   **Communication Liaison, Science Communications Committee**
University of Western Ontario, London, Canada
- Facilitate communication from the Science Faulty to the Chemistry Department at Western University

2015 - Present	**Member, Environment and Sustainability Society**
	University of Western Ontario, London, Canada

- Participate in multiple sustainability initiatives on Western campus

2015 - Present	**Member, Society of Graduate Students Sustainability Committee**
	University of Western Ontario, London, Canada

- Collaborate to accomplish multiple projects to engage graduate students on Western campus

2013 - Present	**Representative, Chemistry Outreach**
	University of Western Ontario, London, Canada

- Supervise labs for high school students

2015	**Science Fair Judge, Seaforth Science Fair**
	Seaforth, Canada

- Directly judged science projects and deliberated with fellow judges to decide on the recipients of the various awards involved

PROFESSIONAL DEVELOPMENT

2016	**Advanced Teaching Program**
	University of Western Ontario, London, Canada

- A hands-on 20 hour seminar over multiple sessions that aims to develop the necessary skills to teach your own course

2014 - Present	**Collaborative Program in Environment and Sustainability**
	University of Western Ontario, London, Canada

- Collaborate with a team to help organize sustainability panel discussions and the annual Earth Day Conference on Western campus

2015	**IMPACT! Sustainability Champions Training Program**
	Natural Step, Guelph, Canada

- A competitive program that provides an intensive 3 day workshop aimed at developing leadership skills and sustainability knowledge

2014`	**The Teaching Mentor Program for Graduate Students**
	University of Western Ontario, London, Canada

- A program where peers supervised me in my natural teaching environment and provided feedback. In addition I evaluated my peers and supplied constructive criticism on their teaching capabilities

Selected Teaching and Learning Workshops
University of Western Ontario, London, Canada

2015	Making the most of your TAship: Educational Leadership and Transferable Skills
	Sustainability at Ivey Conference
	Translating your Idea into a Business Plan
	Careers Outside of Academia
2014	Putting Together a Teaching Dossier
	Writing a Teaching Philosophy Statement
	Encouraging Critical Thinking
	How Do You Know What You Do in Your Classroom Makes a Difference?

AWARDS

2016   **Western Green Award**
- Awarded for work done as part of a team who promoted and initiated composting on campus

2015, 2016   **Excellence Award in the Collaborative Program in Environment and Sustainability**
- Awarded for academic achievement, contribution to the program, and participation in the community

CONFERENCE PRESENTATIONS

2015   **Properties of Carbon Nitride Thin Films Prepared by a Radio Frequency Magnetron Sputtering Deposition Technique**
June 13 - 17, Ottawa, 98th Canadian Chemistry Conference and Exhibition

COURSES COMPLETED AND IN PROGRESS

Fall, 2016   **Geology 9506a: Stable Isotope Geochemistry**....................................IPR

Fall, 2015   **Chemistry 9594A: Materials and Corrosion Processes**........................83

Winter, 2015   **Chemistry 9658Y: Chemistry Seminar**..81

Winter, 2015   **Chemistry 9704B: Solar Energy Conversion**..90

Winter, 2014   **Chemistry 9812B: Condensed Matter Physics**.....................................88